Journal of Palaeogeography, 2023, 12(3): 331–357 (00302)

Available online at www.sciencedirect.com

ScienceDirect

journal homepage: http://www.journals.elsevier.com/journal-of-palaeogeography/

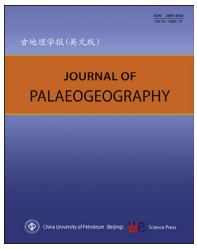

Facies analysis and sedimentary environments

Plio-Pleistocene sedimentation and palaeogeographic reconstruction in the Poso Depression, Central Sulawesi, Indonesia: from a sea channel to a land bridge

Abang Mansyursyah Surya Nugraha [a,d,*], *Ramadhan Adhitama* [b], *Adam D. Switzer* [a,c], *Robert Hall* [d]

[a] *Earth Observatory of Singapore, Nanyang Technological University, 50 Nanyang Ave., 639798, Singapore*
[b] *Fakultas Teknologi Kebumian dan Energi, Universitas Trisakti, Kampus A Gedung D, Jl. Kyai Tapa No. 1, Grogol, Jakarta 11441, Indonesia*
[c] *Asian School of the Environment, Nanyang Technological University, 50 Nanyang Ave., 639798, Singapore*
[d] *SE Asia Research Group, Department of Earth Sciences, Royal Holloway University of London, Egham, Surrey, TW20 0EX, UK*

Abstract The Poso Depression provides a record of Plio-Pleistocene environments and palaeogeography of Central Sulawesi. Outcrop-based sedimentological and provenance studies suggest that during the Pliocene the Poso Depression was a sea channel connecting Gorontalo and Bone bays formed in an asymmetric half-graben. The Pliocene history began with deposition of the Puna Formation with fan deltas at the eastern basin margin and channel complexes in the deep-water basin further east. Analyses of light and heavy minerals indicate the main sediment source was ultrabasic rocks in East Sulawesi with minor and intermittent magmatic and metamorphic input from West Sulawesi. Later, in the Middle to Late Pliocene, carbonates of the Poso Formation accumulated on the eastern basin margin. They are unconformably overlain by shallow marine glaucophane-rich siliciclastics of the Pleistocene Lage Formation that are associated with the rapid exhumation and uplift of the Pompangeo metamorphic complex. This uplift led to the development of a land bridge connecting western and eastern Sulawesi. The terrane evolution favoured increasing the area of exposed land due to rapid tectonic uplift, which when combined with the tropical climate, contributed to faunal speciation and dispersal in Sulawesi.

Keywords Palaeogeography, Poso, Sulawesi, Sedimentation history, Provenance

Received 7 February 2023; revised 27 April 2023; accepted 20 May 2023; available online 23 May 2023

* Corresponding author. Earth Observatory of Singapore, Nanyang Technological University, 50 Nanyang Ave, 639798, Singapore.
E-mail addresses: abang.nugraha@ntu.edu.sg (A.M.S. Nugraha), ramadhan.adhitama@gmail.com (R. Adhitama), aswitzer@ntu.edu.sg (A.D. Switzer), Robert.Hall@rhul.ac.uk (R. Hall).

Peer review under responsibility of China University of Petroleum (Beijing).
https://doi.org/10.1016/j.jop.2023.05.003

1. Introduction

The biodiversity and complex geology of Sulawesi have attracted biologists and geologists to the area since the 19th century (e.g. Müller, 1846; Wallace, 1860, 1863, 1869; Sarasin and Sarasin, 1901). Central Sulawesi includes the collision zone between Sundaland and Australian-origin continental crust of the Sula Spur (Klompé, 1954; Hall, 2012). Wallace (1876) considered the island of Sulawesi "in many respects the most remarkable and interesting in the whole region and perhaps on the globe". Biogeographically, Sulawesi is situated in a transitional zone between faunas of Asian and Australian origin (Heilprin, 1887; Sclater and Sclater, 1899; Dickerson *et al.*, 1928; Darlington, 1957; Holloway and Jardine, 1968; Myers *et al.*, 2000; Procheş and Ramdhani, 2012; Ali and Heaney, 2021), well known as Wallacea (Merrill, 1924). Recent studies have continued to link biogeography to geology (e.g. Michaux, 1994; van den Bergh *et al.*, 2001; Evans *et al.*, 2003a,b,c, 2008; Merker *et al.*, 2009; Stelbrink *et al.*, 2012; Evans, 2012; Driller *et al.*, 2015; Mokodongan and Yamahira, 2015; Nugraha and Hall, 2018; Frantz *et al.*, 2018). The importance of geological events that changed the distribution of land and sea would have influenced climate and the spread and evolution of animals and plants across the island (Nugraha and Hall, 2018; Frantz *et al.*, 2018; Park *et al.*, 2020).

Exposures of metamorphic, magmatic, and ultramafic rocks in the Poso area of Central Sulawesi mark a complex geological suture between the western and eastern parts of Sulawesi (Fig. 1A; Parkinson, 1998; Villeneuve *et al.*, 2001). These rocks are all overlain by the Upper Cenozoic sediments of what is commonly

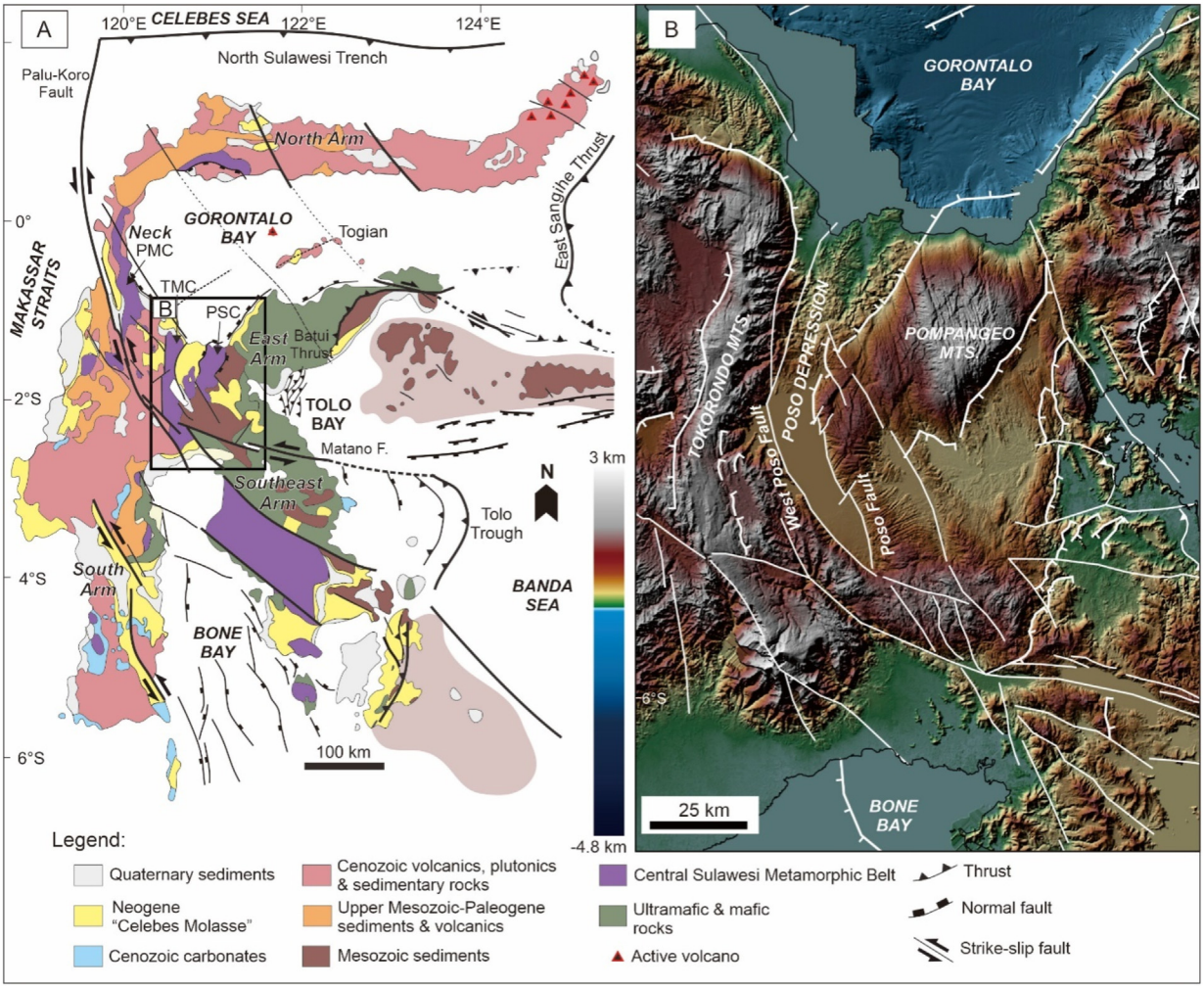

Fig. 1 **A)** Simplified geological map of Sulawesi. Modified after Hall and Wilson (2000), Watkinson (2011). PMC: Palu Metamorphic Complex; PSC: Pompangeo Schist Complex; TMC: Tokorondo Metamorphic Complex; **B)** Shuttle Radar Topography Mission (SRTM) map illustrates the morphology of Poso Depression in the study area.

known as the Celebes Molasse. For biogeographers, Lake Poso, in the centre of the area, is considered an ancient lake ranging from 1 to 30 million years in age, which hosts a highly diverse endemic flora and fauna (van Welzen *et al.*, 2003; von Rintelen *et al.*, 2007; von Rintelen and Cai, 2009; Vaillant *et al.*, 2011; Albrecht *et al.*, 2020). Abendanon (1915) suggested that a transgression of the sea occurred in the Neogene or later, forming the present Poso Depression that was in some way linked to Poso Lake. Our study suggests a more complex history for the area.

2. Geological setting

The study area, referred to here as the Poso Depression, is a geomorphological feature trending roughly north-south and bounded by West Poso and Poso strike-slip faults, which separate a relatively low relief basin from mountains up to 2.550 m to the west and 2.580 m to the east (Fig. 1B and 2A). The Poso Depression is 1.7 km to 35.6 km wide and is about 100 km long. It can be traced across the island from Gorontalo Bay towards mountains at its southern end north of Bone Bay. The Depression itself is underlain by the Central Sulawesi Metamorphic Belt (CSMB) and is overlain by Celebes Molasse (Fig. 1A; Brouwer, 1934; Brouwer *et al.*, 1947; de Roever, 1950, 1956; Audley-Charles, 1974; Sukamto, 1975; Katili, 1978; Hamilton, 1979; Sukamto and Simandjuntak, 1983; Parkinson, 1991,1998). It is bordered by the Cenozoic magmatic belt of western Sulawesi to the west and the East Sulawesi Ophiolite (ESO) to the east. The Poso Depression was interpreted by Parkinson (1991) to have formed by the subsidence of the northern CSMB, which exposed the Pompangeo Schist Complex (PSC), as a foreland depression or crestal collapse graben following the collision of the Sula Spur and western Sulawesi. Villeneuve *et al.* (2001) interpreted a Poso Lake graben related to a mid-Pliocene tectonic event. Spencer (2010, 2011) suggested that the domal landforms of the Tokorondo and Pompangeo Mountains on the western and eastern sides of Central Sulawesi are active or recently active metamorphic core complexes with their upper surfaces being gently dipping detachment faults (Fig. 2A). This tectonic interpretation is supported by offshore seismic lines in the Poso Basin of southern Gorontalo Bay (Pezzati *et al.*, 2014).

The northern part of CSMB is widely known as the Pompangeo Schist Complex (PSC) and contains two metamorphic units, both considered to be subduction related. The western unit is a Cretaceous accretionary assemblage (Parkinson, 1991, 1998) and the eastern unit is an Oligo-Miocene subduction complex (Helmers *et al.*, 1989; Wijbrans *et al.*, 1994; Parkinson, 1996; Mawaleda *et al.*, 2018). The metamorphic rocks and deformed Mesozoic sediments including the Cretaceous Matano Formation are overlain by the Celebes Molasse (Fig. 2A; Koolhoven, 1930; Sukamto and Simandjuntak, 1983; Parkinson, 1991, 1998). A variety of poorly dated sediments that have been assigned to the Celebes Molasse (Sarasin and Sarasin, 1901) have been widely interpreted as post-orogenic rocks deposited after a major collision (van Bemmelen, 1949; Kündig, 1956; Villeneuve *et al.*, 2001). In the Poso Depression, the PSC is directly overlain by Mio-Pliocene clastic sediments of the Puna Formation and Plio-Pleistocene reef limestones of the Poso Formation (Simandjuntak *et al.*, 1997; Parkinson, 1998). These sediments were assigned to the Celebes Molasse (e.g. van Bemmelen, 1949; Kündig, 1956; Milsom *et al.*, 1999), but recent studies have shown that the ages and sedimentation history of the Celebes Molasse varies across Sulawesi (Hall and Wilson, 2000; Nugraha and Hall, 2018).

A revised stratigraphy of the Celebes Molasse defined two new units, the Tambarana and Lage formations (Fig. 2B; Nugraha *et al.*, 2022), and integrated them with the previously recognised Puna and Poso formations (Rusmana *et al.*, 1993; Simandjuntak and SuronoSupandjono, 1997; Parkinson, 1998). This study reports new results based on a field-based investigation of the Plio-Pleistocene sedimentary rocks in the Poso Depression, which aimed to define their sedimentation history, provenance, and palaeogeography.

3. Data and methodology

3.1. Sedimentology

In many parts of Sulawesi, Neogene sedimentary rocks are absent or exposures are limited by the dense vegetation in the tropical setting. Fortunately, new exposures created during recent road construction provided fresh rocks and new information. Field observations were carried out at 55 localities (Fig. 2A; Supplementary Data 1) where sedimentological and stratigraphic observations were made. Lithological observations are summarised in Table 1. This study also makes reference to biostratigraphic age ranges from Nugraha *et al.* (2022; Supplementary Data 2).

3.2. Petrography

Medium-to coarse-grained sandstones were collected for petrographic analysis. Line point-

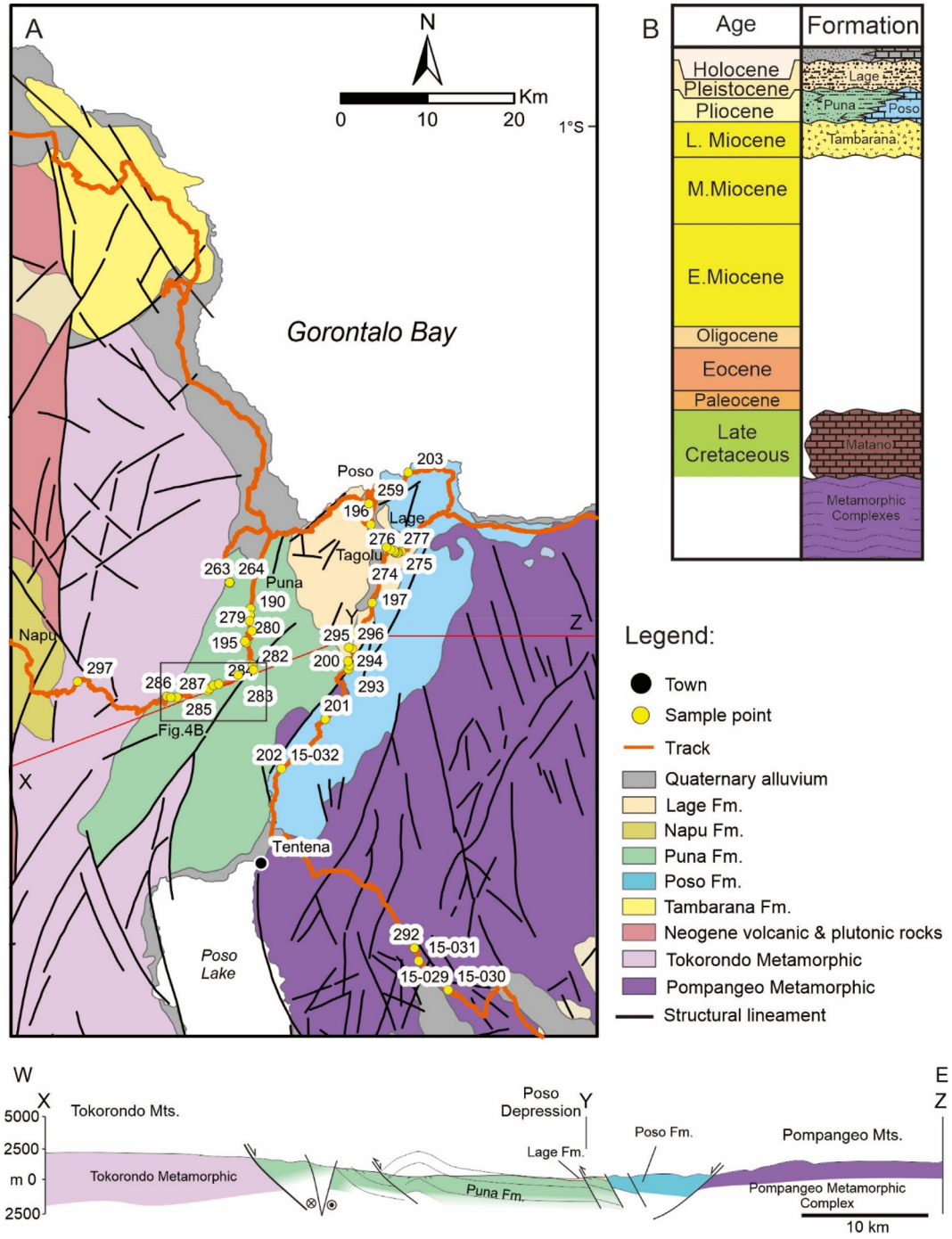

Fig. 2 **A)** Geological map of Central Sulawesi (modified from Simandjuntak *et al.*, 1997). Revision was made in areas where observations were made. Cross-section X-Y-Z across the Tokorondo Metamorphic complex, Poso Depression and Pompangeo Schist Complex; **B)** Revised stratigraphy of Central Sulawesi (modified from Nugraha *et al.*, 2022).

counting (Galehouse, 1971) was performed using the Gazzi-Dickinson method and at least 400 grains were identified for each sample (Supplementary Data 3). Sandstone compositions were plotted using quartz-feldspars-lithic fragments (QFL) and monocrystalline quartz-feldspars-total lithic fragments (QmFLt) diagrams followed conventions of Dickinson (1970, 1985), Dickinson and Suczek (1979), Dickinson *et al.* (1983), Ingersoll (1983), and Dorsey (1988).

3.3. *Heavy minerals*

Sandstone samples were processed using standard heavy mineral separation methods of Mange and

Table 1 Facies association and environmental interpretation for the Puna, Poso, and Lage formations.

Formation	Facies association	Facies description	Main characteristic	Interpretation
Puna Formation	Facies Association Puna 1 (FAP1)	Normally graded conglomerate, clast-supported conglomerate, matrix-supported conglomerate, horizontally-stratified conglomerate, normally graded sandstone, horizontally-stratified sandstone, planar cross-stratified sandstone, trough cross-stratified sandstone and massive mudstone.	Coarse grained deposits with well-developed normal grading, inverse grading, and bipartite discontinuities.	Delta foreset
	Facies Association Puna 2 (FAP2)	Clast-supported conglomerate, matrix-supported conglomerate, normally graded conglomerate, inversely graded conglomerate, horizontally-stratified conglomerate, massive sandstone, horizontally-stratified sandstone, and rippled sandstone.	A wide textural range of conglomerates, from poorly sorted and chaotically to well sorted clast-supported conglomerate and thick sandstone beds.	Submarine channel-fill
	Facies Association Puna 3 (FAP3)	Massive sandstone, normally graded sandstone, rippled sandstone, horizontally laminated fine-grained sediment, massive mudstone, contorted bioclastic limestone, and subsidiary massive conglomerate and normally graded conglomerate.	Ta,c,d,e sandstones and silty mudstones, muddy debris flow deposits, and mass movement facies.	Levee and overbank
Poso Formation		Grainstones, packstones, wackestones, floatstones, and rudstones.	Massive to bedded limestones that include grainstones, packstones, wackestones, floatstones, and rudstones.	Shallow marine reef platform
Lage Formation	Facies Association Lage 1 (FAL1)	Planar and wavy laminated sandstones, massive mudstones, horizontally laminated mudstones, bioturbated mudstones, and grainstones (limestone).	Coarsening upwards from mudstone to interbedded sandstone and mudstone with limestone intercalations.	Offshore transition
	Facies Association Lage 2 (FAL2)	Clast- to matrix-supported conglomerates and interlaminated mudstones, siltstones, and very fine-grained sandstones.	Slumped conglomerate, sandstone, and mudstone beds that are confined between undisturbed FAL1 beds.	Slump

Maurer (1992) to obtain 300 g of 63—250 μm dry and clean fractions (Supplementary Data 4). Selected samples were crushed, decarbonated in 10% acetic acid, wet and dry sieved (63—250 μm meshes sieving stack), and separated in a funnel using lithium polytungstate (LST, at a density of 2.89 g/cm^3). Grains were identified using an optical polarising microscope (NIKON Eclipse Lv 100) with a ribbon counting method (Galehouse, 1971). Additional Scanning Electron Microscope (Hitachi S3000 SEM) and Energy Dispersive Spectroscopy (EDS, X-MaxN 50-silicon drift) analyses were performed to establish and/or confirm the identity of some heavy minerals.

3.4. Zircon geochronology

The heavy mineral fraction of sample ES14-67 was processed using Frantz magnetic separation, diiodomethane (DIM, at a density of 3.3 g/cm^3) heavy liquid separation, and zircon picking (using an Olympus SZx12 binocular microscope). Zircons were mounted in araldite resin blocks, polished and cathodoluminescence (CL) images were made using Hitachi S3000 SEM-CL. Laser ablation inductively coupled plasma mass spectrometry (LA-ICP-MS) dating of zircons was performed on a New Wave NWR 213 nm laser ablation system coupled to an Agilent 7700 quadrupole-based ICP—MS at Birkbeck College, University of London. The Plešovice zircon standard (337.13 ± 0.37 Ma; Sláma *et al.*, 2008) and a NIST 612 silicate glass bead (Pearce *et al.*, 1997) were used to correct for instrumental mass bias and depth-dependent inter-element fractionation of Pb, Th, and U. Data reduction and common lead correction were performed using GLITTER™ software (Griffin *et al.*, 2008) and Andersen (2002) methods. Concordant ages were accepted based on a 10% threshold (Supplementary Data 5). In this study, the youngest zircon grains in samples were used to constrain the maximum depositional age (MDA) of the samples (e.g. Nelson, 2001; Fedo *et al.*, 2003; Andersen, 2005).

4. Results and interpretation

4.1. Field descriptions

Lithological observations were assigned to groups of sedimentary facies called Facies Associations (FA) that represent a particular sedimentary environment based on the sedimentology and dominant sedimentary structures identified in outcrops (Table 1). Field descriptions of the stratigraphic units are also illustrated in this section.

4.1.1. Puna Formation

The Puna Formation is exposed on the western and eastern sides of the Poso Depression. In the west, rocks are exposed along the trans-Sulawesi Road that crosses the Tokorondo Mountains. Puna Formation sediments in the west are dominated by coarse-grained deposits of conglomerate and sandstone that were assigned to Facies Association Puna 1 (FAP1). To the east of Poso Depression and on the road from Poso to Tentena, sedimentary rocks are finer and are dominated by sandstones and mudstones of Facies Association Puna 2 (FAP2) and 3 (FAP3). Detailed observations of lithofacies and abbreviations for different facies in the Puna Formation are summarised in Table 2.

4.1.1.1. Facies Association Puna 1 (FAP1): delta foreset. At the measured stratigraphic section of the FAP1, we examined a total thickness of 32 m of coarsening-up foreset deposits (Fig. 3). The FAP1 facies can be further subdivided into lower (foreset deposits 1 and 2), middle (foreset deposits 3 to 7), and upper (foreset deposits 8 and 9) parts. The lower part is dominated by a prominent fining-up sequence of facies Gn, Gc, Sn, and Fm (Fig. 3). The erosive basal bed is dominated by cobble conglomerates that include rip-up clasts of mudstones. Sedimentary structures characteristic of the lower FAP1 facies include normally graded, cross- and parallel stratification. Mudstone beds are very thin (<20 cm) and are commonly eroded by successive coarser beds. Rip-up clasts of underlying mudstones are commonly incorporated into the coarser channel beds above. Sample ES13-267 from one of the mudstone beds in FAP1 contains benthic foraminifera *Cibicides* sp., *Eponides* sp., and *Bolivina* sp.

The middle part of the foreset beds sequence consists of (1) fining-up succession of facies Gc, Gn, Sp, and St, (2) coarsening-up facies Sm, Sh, Gm, and Gi, and (3) interstratified facies Sh, Gh, Gm, and Gc (Fig. 3). Sedimentary structures here include normally graded, inversely graded, and bipartite deposits of matrix-supported conglomerates and sandstones. Cross-stratifications though infrequent suggest northwestward palaeocurrents. Bedding generally exhibits a strong down-transport wedging geometry. Outsized clasts were observed within some of the amalgamated sandstones and conglomerate beds. Conglomerate beds locally pinch-out down-slope toward the west. Upper bed boundaries range from sharp to gradational contacts and low relief scoured bases occur locally.

The uppermost part of the foreset sequences is characterised by interstratified conglomerates and conglomeratic to pebbly sandstones that consist of

Table 2 Sedimentary facies for the Puna Formation.

Facies name	Bed thickness, geometry, bounding surfaces	Description	Depositional processes
Clast-supported conglomerate (Gc)	Centimetre- to metre- thick. Beds are massive and occasionally have stringer geometry. Upper and lower bed boundaries show flat- and erosive surfaces respectively.	Black to greenish-brown, clast-supported, moderate to well-sorted, sub- to well-rounded conglomerates. Matrix is coarse- to very coarse-grained serpentinite-rich sand. Clast consists of ultrabasic, basic rocks, serpentinite, chert, gabbro, dolerite, minor schists and gneiss, green sandstones, siltstones, and limestones. Clast size ranges from pebble to boulder.	The clast-supported conglomerate implies interstices filling by matrix following deposition (Miall and Gibbling, 1978; Miall, 1977, 2014).
Matrix-supported conglomerate (Gm)	Centimetre-to metre-thick. Massive but sometimes occurs as lenses or pockets in massive and amalgamated conglomerate beds. Sharp upper and lower boundaries.	Greenish dark grey to greenish-brown, matrix-supported, poorly sorted, sub-to well-rounded conglomerates. Matrix is coarse- to very coarse-grained serpentinite-rich sand. Clast size ranges from granule to boulder. Clasts include ultrabasic, basic rocks, serpentinite, chert, gabbro, dolerite, minor schists and gneiss, sandstones, siltstones, and limestones. Medium to very coarse sand matrix. Crude horizontal bedding, weak grading and lateral fining were observed.	Sediment gravity flow (cohesive - debris flow; Lowe, 1982; Mulder and Alexander, 2001)
Normally graded conglomerate (Gn)	Up to 2 m thick. Sheet geometry. Upper contacts are gradational, while the lower contacts are planar or erosive.	Black to greenish-brown, clast-supported, moderate to well-sorted, normally graded, sub- to well-rounded conglomerates. Matrix is medium- to very coarse-grained serpentinite-rich sand. Mud clasts are commonly observed at the base.	Waning turbidity current or turbulent flow (Lowe, 1982; Postma *et al.*, 1988)
Inversely graded conglomerate (Gi)	Centimetre-to metre-thick. Lenticular geometry. Sharp to gradational boundaries.	Black to greenish-brown, clast-supported, moderate to well-sorted, inverse graded, sub- to well-rounded conglomerates. Matrix is medium- to very coarse-grained serpentinite-rich sand. Clast size is generally smaller than Gc and ranges from granule to cobble. It may contain floating pebbles to cobbles.	Dispersive pressure of grain and clast interaction that promotes flow strength and buoyant lift (Surlyk, 1978; Shanmugam, 1997).
Horizontally-stratified conglomerate (Gh)	Centimetre-to metre-thick. Sheet geometry. Sharp to gradational boundaries.	Gh is characterised by crude parallel horizontal lamination due to clast arrangement. Elongate clasts commonly exhibit a planar horizontal alignment or a crude imbrication. Clast size ranges from boulder to pebble. Matrix is medium- to very coarse-grained serpentinite-rich sand. Beds have distinct boundaries if there are significant clast size differences between layers, for example a sudden change from boulder or cobble to pebble or granule and sand.	Gh suggests laminar flow deposition (Fisher, 1971). Alternatively, it can also be formed by freezing near the top of inertia-flow layer (Postma *et al.*, 1988).
Massive sandstone (Sm)	Millimetre- to metre thick. Sheets and lens geometries. Upper boundaries are horizontally sharp, while lower boundaries are planar or erosive.	Dark green to greenish-brown and light grey, moderate to well-sorted, sub-angular to sub-rounded grain, massive, pebbly- to medium-grained sandstones. Grains consist of serpentinite, quartz, and mafic minerals.	Sandy debris flow and/or sediment gravity flow (high-density turbidity current; Postma *et al.*, 1988)

(*continued on next page*)

Table 2 — (*continued*)

Facies name	Bed thickness, geometry, bounding surfaces	Description	Depositional processes
Normally graded sandstone (Sn)	Centimetre- to metre-thick. Sheets and lens geometries. Planar and erosive bases, while tops are sharp to gradational.	Dark green to greenish-brown and light grey, moderate to well-sorted, sub-angular to sub-rounded grain, normally graded, coarse- to medium- and fine- grained sandstones. Grains consist of serpentinite, quartz, and mafic minerals. Some thicker beds show pebbly to granule sandstones at the base. Pebbles and granules are dominated by ultrabasic and basic rocks.	Decelerating turbulent flow or turbidity currents (Lowe, 1982; Postma *et al.*, 1988; Mulder and Alexander, 2001).
Inversely graded sandstone (Si)	Centimetre-thick. Sheet and lens geometries. Sharp bases and gradational to sharp tops.	Dark green to greenish-brown and light grey, moderate to well-sorted, sub-angular to sub-rounded grain, inversely graded, very fine- to coarse- grained and pebbly sandstones. Grains consist of serpentinite, quartz, and mafic minerals. Pebbles and granules are dominated by ultrabasic and basic rocks.	Traction carpets in high density turbidity currents (Lowe, 1982). Alternatively, it can also be produced by debris flows (Shanmugam, 1997, 2000).
Horizontally-stratified sandstone (Sh)	Centimetre-thick. Sheet and lens geometries. Bases are planar to gradational and the top is sharp.	Greenish black to greenish-brown and light grey, moderate to well-sorted, sub-angular to sub-rounded grain, horizontally to sub horizontally stratified, fine-to very coarse-grained sandstones. Grains consist of serpentinite, quartz, and mafic minerals.	Rolling and saltation of grains along the surface under low flow velocities and no flow separation conditions (lower flow regime) or from washed out ripple and dune bedforms when the flow is suppressed at higher velocity (upper flow regime; Nichols, 2009).
Planar cross-stratified sandstones (Sp)	Millimetre- to centimetre- thick. Sheet and lenses geometries. Sharp upper and lower boundaries.	Dark green to greenish-brown, poorly to well-sorted, sub- to well-rounded, planar cross-stratified, fine grained- to pebbly and conglomeratic sandstones. Angle of cross-beds ranges from 20° to 40°.	Migration of transverse dunes formed under bed shear stress exerted by unidirectional traction currents (Collinson, 1996; Miall, 1996; Hjellbakk, 1997).
Trough cross-stratified sandstones (St)	Centimetre- to metre- thick. Sheet geometry. Sharp tops and sharp or erosive lower boundaries.	Dark green to greenish-brown, poorly to well-sorted, sub- to well-rounded, trough cross-stratified, fine grained- to pebbly and conglomeratic sandstones. Angle of cross-stratifications ranges from 10° to 35°.	Migration of sinuously-crested dunes formed under bed shear stress exerted by unidirectional traction currents (Nichols, 2009).
Rippled sandstone (Sr)	Centimetre-thick. Sheet and lenses geometries. Sharp top and bases	Dark green to greenish brown, moderate to well-sorted, sub-to-well rounded, rippled, fine- to medium-grained sandstones.	Migration of linguoid ripples by low-energy unidirectional traction currents (Miall, 2010).
Horizontally laminated fine-grained sediments (Fh)	Millimetre- to centimetre- thick. Sheet geometry. Sharp upper and lower boundaries.	Dark grey to black, poorly to moderate-sorted, sub- to well-rounded, horizontally planar, thinly bedded fine- to very fine-grained sandstones to mudstones. Mudstones and siltstones are highly calcareous and conserve rarely leaf fossil. Sandstones contain plant debris and mud granules. Fh may laterally shift into wavy lamination.	Low density turbidity currents (Nichols, 2009). The presence of plant debris and leaf fossils suggest a terrigenous source.

Wavy laminated fine-grained sediments (Fw)	Millimetre- to centimetre- thick. Sheet geometry with limited lateral continuity. Sharp upper and lower boundaries.	Dark grey to black, poorly to moderate sorted, sub- to well-rounded, horizontally planar, thinly bedded fine- to very fine-grained sandstones to mudstones. Fw can laterally shift into horizontally planar fine-grained sediments. Fine-grained sandstones confined in discontinuous wavy interbedded mudstones show pinch-out and lenticular geometry. Beds have irregular shapes, wavy, and lenticular laminations.	Lateral changes of Fh into Fw may be produced by an increase of bottom currents' energy (O'Brien, 1996). Sand breaks between laterally discontinued mudstone beds may indicate water-escape structures. This condition is possibly caused by escaping trapped water in permeable unit (sandstone) through capped impermeable mudstone during consolidation of sediment (Pickering *et al.*, 1986; Shanmugam, 2000).
Massive mudstones (Fm)	Millimetre- to centimetre- thick. Sheet geometry. Sharp upper and lower boundaries.	Grey to black, millimetre- to centimetre- thick beds of interbedded claystone, siltstone, and fine- to very fine-grained sandstone. Some scours and load casts occur at the top of Fm beds. Rarely observed bioturbation of horizontal trace fossil. Bioturbation index 0 to 2, *Skolithos*.	Low-energy deposition by suspension settling and dilute low-density turbidity currents (Nichols, 2009).
Contorted bioclastic limestone (Lc)	Centimetre- thick. Tops are sharp while bases are erosive.	Wackestone to grainstone that consists of bioclastic materials (i.e. broken shells, broken corals, foraminifera and red algae), angular quartz, and mud clasts. Internal geometry shows folded layers that is underlain by normally graded unit. Various fold types occur, from symmetrical, asymmetrical, and overturned folds.	Highly folded strata indicate gravity-controlled unconsolidated sediment deformation like slumping (Pickering *et al.*, 1986).

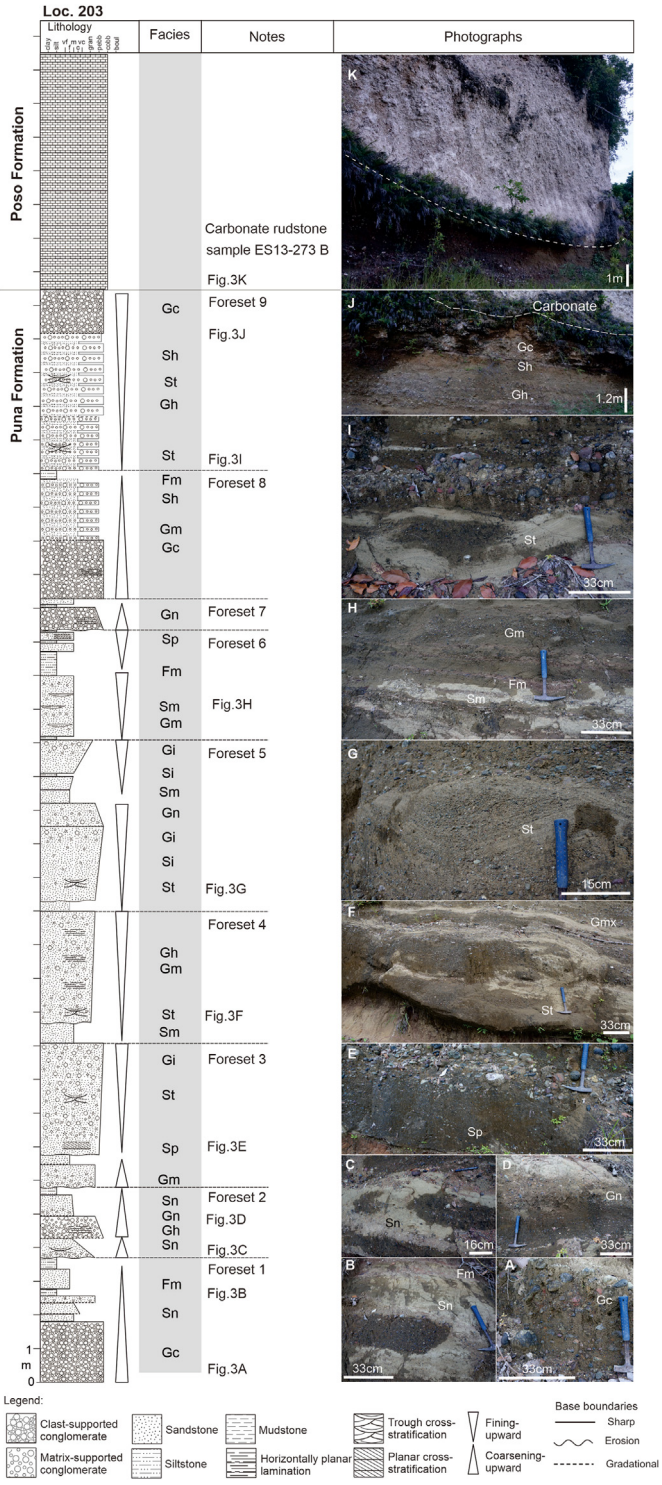

Fig. 3 Measured stratigraphic section of the Puna Formation in eastern Central Sulawesi is situated at location 203 (details in Supplementary Data 1). Note the stratigraphic contact between the Puna Formation and overlying Poso Formation at the top of logged section. The facies code used in the column can be found in Table 1. Field photographs (**A**) clast-supported conglomerate; (**B**) normally graded conglomerate that is overlain by massive mudstone; (**C**) normally graded sandstone; (**D**) normally graded conglomerate; (**E**) planar cross-stratified conglomerate with clast-supported conglomerate on top; (**F**) trough cross-stratified sandstone and matrix-supported conglomerate; (**G**) trough cross-stratified pebbly sandstone; (**H**) interbedded massive sandstone, massive mudstone, and matrix-supported conglomerate; (**I**) trough cross-stratified sandstone; (**J**) interbedded horizontally stratified conglomerate, horizontally-stratified sandstone, and clast-supported conglomerate that are overlain by limestone of the Poso Formation; (**K**) Position of the boundary between the Puna Formation and overlying Poso Formation is depicted in dashed line.

rhythmic facies of Sh, Gh, Gm, Gc, St, and minor Fm (Fig. 3). Interstratified facies Sh and Gm occasionally develop to horizontally planar sedimentary structures with normal, and inverse grading. Facies Gc and St commonly appear as irregular and lenticular beds. Although bedding contacts are difficult to identify in this unit, low relief scoured trough beds were identified in several locations. Amalgamated conglomerate and sandstone beds are laterally continuous for tens of meters and commonly have a minimum thickness of 2 m. Matrix-supported conglomerates often pass laterally down-slope into well-defined bipartite deposits.

Collectively, the FAP1 facies association is characterised by coarse-grained deposits with well-developed normal grading, inverse grading, and bipartite discontinuities. It likely indicates deposition by gravelly high-density turbidity currents and debris flows. Where found, normal grading is likely the product of a waning turbulent flow or turbidity currents from which deposition of coarse-grained material is followed by finer-grained material. Rare cross-stratifications are also interpreted to be formed by turbulent flow. Inverse grading noted in the sequence likely resulted from increased dispersive pressures in the gravel traction carpet, where the coarse-grained fraction settled into the basal layer to form a gravel traction carpet with an overflowing sandy turbulent suspension (e.g. Lowe, 1982; Postma *et al.*, 1988). Increased dispersive pressures in the gravel traction carpet can cause inverse grading (Lowe, 1982). Outsized clasts are interpreted to be transported along the rheological interface between the basal inertia flow (traction carpet) and the lower-density faster-moving turbulent over-flow (Postma *et al.*, 1988). Pinch-out of the conglomerate bed indicates rapid *en masse* deposition of gravel layers by frictional freezing. Lenses of conglomerates and sandstones might represent erosional lags, gully, and shallow channel fills.

Bipartite discontinuities indicate deposition by a high-density turbidity current comprising a gravel traction carpet with an overflowing sandy turbulent suspension (Lowe, 1982; Postma *et al.*, 1988). The large disparity in clast sizes suggests that rapid clast segregation would have occurred if the flow had been turbulent (e.g. Falk and Dorsey, 1998). Sandstones and mudstones that were deposited sharply on coarse-grained pebbly sandstone and conglomerates likely indicate turbidites that are often entrained on top of subaqueous debris flows (Nemec and Steel, 1984; Postma *et al.*, 1988). Preserved benthic foraminifera support the interpretation of subaqueous deposition in a shallow marine environment.

In summary, upper foresets record the deposition of predominant cohesionless debris flows, while the lower foresets record deposition of prevalent high-density turbidity currents and the development of gravel traction carpets. These indicate rapid input of coarse-grained materials from the fluvial channels into the downslope foreset of a Gilbert-type fan delta (e.g. Falk and Dorsey, 1998; Gobo *et al.*, 2015).

4.1.1.2. Facies Association Puna 2 (FAP 2): submarine channel-fill. The submarine channel-fill facies association can be subdivided into a lower sequence (1) of conglomerate- and an upper sequence (2) of sandstone-rich units. A general fining-up characterises the conglomerate-rich channel-fill and includes amalgamated conglomerates of facies Gc, Gm, Gn, Gi, Gh, and subordinate sandstones of facies Sm, Sh, and rarely Sr (Fig. 4). Sub-to well-rounded conglomerate clasts in this facies consist of predominant ultramafic and mafic rocks with minor green siltstones (Fig. 5A). Matrix-supported conglomerates and pebbly sandstones commonly occur as irregular stringers and lenses. The conglomerates exhibit shallow scoured bases and have beds which are commonly 1—10 m thick, but amalgamated beds of the conglomerates make individual bed observation difficult. Rare thin fine-grained and fractured siltstone layers are locally present below the sharp conglomerate base and may represent a sheared layer.

Sandstone proportion increases upward in the FAP 2 facies with bed thicknesses ranging from 0.2 to 3 m. Sandstone-rich units consist of fining-upward facies Sm, Sn, and subsidiary facies Fh (Fig. 5B). The upper parts of this facies association contain Ta,b sandstones that are interbedded with thin sandstones and mudstones. Sandstone beds have a relatively constant thickness and form sheet-like bodies. Normally graded sandstones are common with bed thicknesses ranging between 0.4 and 3 m. Load casts, flame structures, and rip-up mudstone clasts often appear at the sandstone bases. Rare mudstone clasts float in sandstone beds.

The FAP 2 facies association suggests initial channel filling by clast-supported conglomerates and final filling of thick-bedded sandstones. Channel filling generally involves a waning of gravel-laden turbidity current activity and/or decrease in flow competence (e.g. Bernhardt *et al.*, 2011). The conglomerate unit likely represents the initial influx of the coarse-grained detritus into the Poso Depression during the deposition of the Puna Formation in a submarine channel. Erosive bases are indicative of several individual channels that

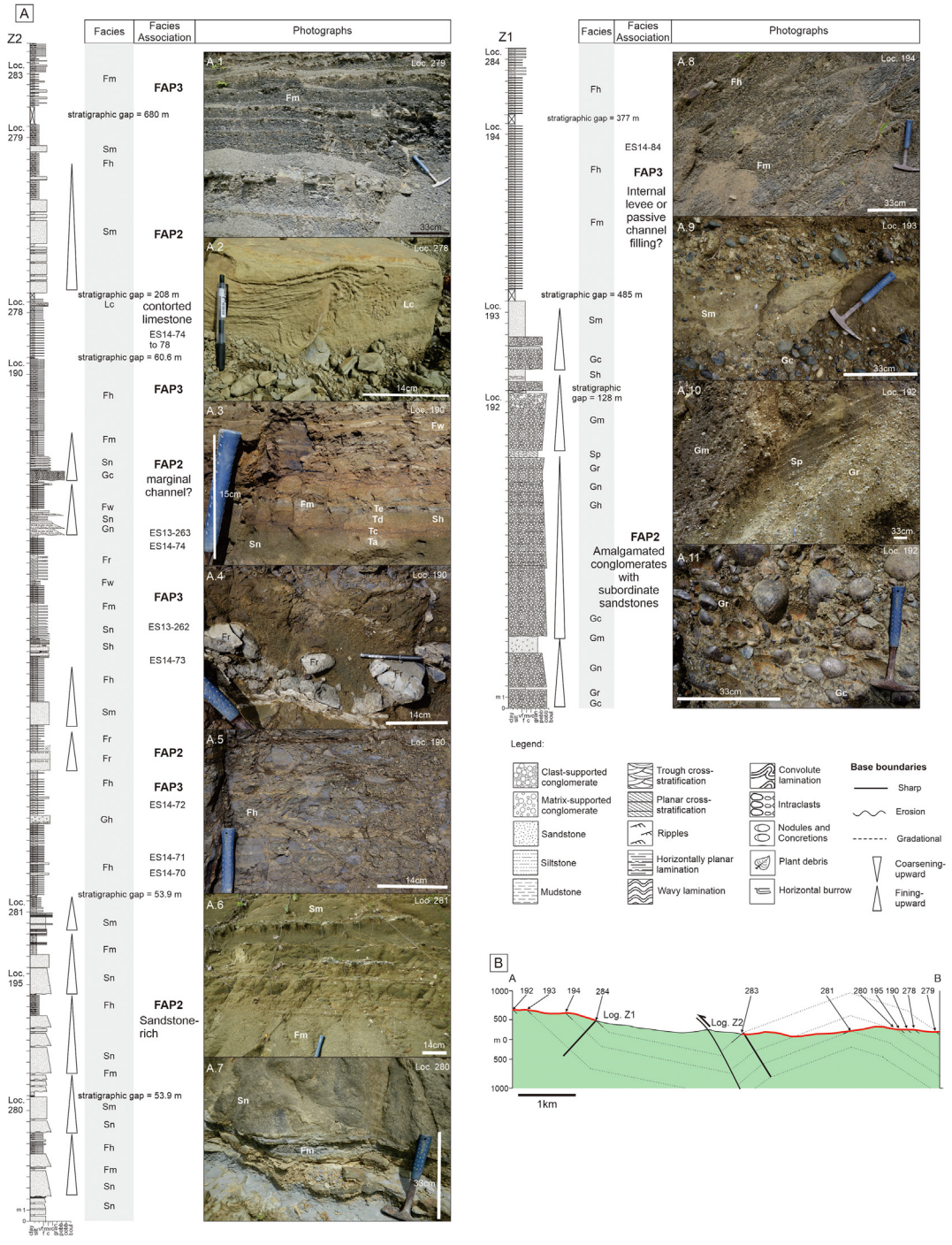

Fig. 4 **A)** Stratigraphic logs (Z1 and Z2) for the Puna Formation in western Central Sulawesi based on (**B**) reconstructed geological cross-section from the site locations along the road from Poso to Napu. The facies code used in the columns can be found in Table 1. Field photographs of (**A1**) massive mudstones; (**A2**) contorted limestone bed; (**A3**) almost complete Bouma Sequence Ta, Tc, Td, Te; (**A4**) parallel rafted blocks or clasts in mudstone beds; (**A5**) horizontally laminated fine-grained sediments; (**A6**) interbedded massive mudstone and sandstone; (**A7**) normally graded sandstone on top and massive mudstone below; (**A8**) interbedded horizontally laminated fine-grained sediments and massive mudstone; (**A9**) clast-supported conglomerate and massive sandstone; (**A10**) interbedded inversely-graded conglomerate, massive conglomerate, and planar cross-stratified sandstone; (**A11**) amalgamated clast-supported conglomerate with inversely-graded conglomerate. Detailed site locations are listed in Supplementary Data 1.

form a channel complex. Unfortunately, no lateral evidence of separate channels was observed in the field. A wide textural range of conglomerates, from poorly sorted and chaotic to well-sorted matrix-supported and clast-supported types indicates an early-stage channel-complex set (e.g. Kneller *et al.*, 2020).

Fig. 5 **A)** Complex amalgamated conglomerates of the Puna Formation; **B)** Sandstone dominated-interbedded sandstone and mudstone of the Puna Formation; **C)** Mudstone-dominated interbedded mudstone and sandstone and interbedded mudstone and sandstone with subsidiary conglomerate and rafted deposits (white arrows) of the Puna Formation; **D)** Massive outcrop of the Poso Formation consists of mainly rudstone, floatstone, and packstone in a quarry near Tentena; **E)** Slumped shelfal slope deposits (FAL2) of the Lage Formation and the lower part includes clast-to matrix-supported conglomerates and interlaminated mudstones, siltstones, and very fine-grained sandstones. In the upper part, offshore transition deposits (FAL1) consist of planar horizontally and wavy laminated sandstones, massive mudstones, horizontally laminated mudstones, bioturbated mudstones, and grainstones (limestone); **F)** Mudstone bed of the Lage Formation contains *Rosselia* (upper right arrow) and *Thalassinoides* (lower left arrow) that indicate a shallow marine environment; **G)** Folded beds consist of interbedded conglomerates, sandstones, and mudstones. Coordinate locations can be found in Supplementary Data 1.

Graded, well-sorted, imbricated conglomerates suggest deposition of single event turbidity currents. Matrix-supported conglomerates are indicative of subordinate debrites in the early-stage fills. Cross-stratification in the conglomerate beds suggests bed-load transport in the channel (Beaubouef, 2004). Lenticular and isolated coarse sandstones indicate widespread and frequent erosion in a high-energy environment (Bernhardt *et al.*, 2011).

A noticeable increase in sandstone thickness in the upper part of the logged section is indicative of deposition by debris flows and later reworking and winnowing by turbidity currents along the channel axes (Winn and Dott, 1979). Mudstone clasts commonly float in the debris flows. The thick sandstone beds are interpreted to have been deposited during sand-rich, distributive stage of channel-complex development. Ta,b sandstones with minor cross-stratification in the upper sandstone-rich unit indicate deposition from the suspended load of through going flows at channel margins (Beaubouef, 2004).

4.1.1.3. Facies association Puna 3 (FAP3): levee and overbank facies. This facies association consists of facies Sm, Sn, Sr, Fh, Fw, Lc, and Fm with subsidiary facies Gm and Gn (Fig. 4A). FAP3 is characterised by continuous, fine-grained sediments, with occasional thickly-bedded (0.3—1 m) channelised sandstones. The sandstones are either massive or normally graded and they commonly have a sharp contact with mudstones. Partial Bouma Sequences (Ta, Tc, Td, Te) occur rarely within the succession with some soft-sediment deformation structures (Fig. 4A3). They are commonly associated with erosional surfaces, chaotic beds, and debris-flow deposits. FAP3 has a lower sandstone proportion compared to FAP2.

Thinly interbedded sandstone and mudstone is often separated by isolated and rafted clasts of discontinuous sandstone, siltstone, and claystone beds that are parallel to bedding (Figs. 4A4 and 5C). The claystone and siltstone beds exhibit parallelly rafted blocks or clasts (arrows in Fig. 5C). Some of the isolated mudstone blocks look laterally detached from the more continuous beds. Sandstone clasts vary in grain size (fine sand to pebble), shape (rounded to angular) and size (pebble to boulder). Unlike mudstone, sandstone clasts are more isolated and disoriented, although they are still roughly parallel to the main bedding. Small-scale soft-sediment deformation with water escape structures appears locally. Interbedded mudstone is commonly interrupted by thin structureless sandstone, rippled sandstone, and less commonly normally graded sandstone. Calcareous nannofossils and foraminifera (Supplementary Data 2) were rarely found in the mudstones. Chaotic deposits of contorted limestone (facies Lc; Fig. 4A2) and brecciated mudstone also appear rarely in interbedded mudstone.

The presence of alternating sandstone and mudstone in the FAP3 facies association is interpreted as levee and overbank turbidites. Lithofacies in the interchannel areas include thin-bedded turbidites of that are characterised by interbedded Ta,c,d,e sandstones and silty mudstones, muddy debris flow deposits, and mass movement facies. The almost complete Bouma Sequence is indicative of turbidity currents product (Shanmugam, 2000), in contrast to the FAP2 that was deposited from energetic, high-concentration sediment flows. Sediment deposition was initiated when the competence of the flow reduced as the flow overspilled the levee crest and became unconfined, and rapidly decelerated (Hiscot *et al.*, 1997; Kane *et al.*, 2010). Particles with higher settling velocities, such as sand, were deposited first as the decelerating current spread over the levee, whilst clay remained in suspension until the flow was almost at rest (McCave, 1975; Lowe, 1982; Hiscott, 1994; Kneller, 1995; Kneller and McCaffrey, 2003; Hansen *et al.*, 2017). Massive sandstones and traction-dominated sedimentary structures such as ripples are also common in the proximal external levee (Hansen *et al.*, 2017). Thickness of sandstone beds generally decreases away from the channel, in contrast to mudstone beds (Kane *et al.*, 2007). Nannofossil and foraminifera assemblages indicate an open marine and Pliocene age (Supplementary Data 2; Nugraha *et al.*, 2022). Contorted limestone identified in FAP3 might represent remobilised deposits within the slope of a levee. Rafted clasts are interpreted to be slide- and debris-flow products that might also be associated with gravity induced tectonics (Shanmugam, 2000).

4.1.2. Poso Formation

The Poso Formation consists of carbonates which are mainly exposed in the eastern part of the Poso Depression (Fig. 2A). This formation has an estimated total thickness of about 250 m based on measured sections and reconstructed cross-sections. The thickest section observed in the field is about 10 m. Individual beds have thicknesses between 0.6 and 1.2 m, with bedding dips between 22° and 82°. They consist of massive to bedded limestones that include grainstones, packstones, wackestones, floatstones, and rudstones (Fig. 5D). The wackestone to grainstone carbonates are composed of large benthic foraminifera, encrusting red algae, echinoid spines, bivalve, gastropod, and coral fragments with minor quartz. In

contrast, the rudstones and floatstones are dominated by fragments of branching, platy, and domal corals. These corals are enclosed by a packstone to grainstone matrix.

The rudstone and floatstone of the Poso Formation are likely the product of proximal to distal reef flank and fore reef deposits. Rudstone is usually deposited close to the reef crest whereas wackestone, packstone, and grainstone usually indicate a low, moderate to high-energy setting that might develop in an inner platform, platform margin, or interstices between coral framework environments (Wilson, 1975). Based on the identification of materials that were mainly deposited in the rudstone, coral fragments must have been derived from a reef crest to reef front area. Foraminifera assemblages from the carbonates of the Poso Formation indicate a shallow marine environment and a Pliocene age (Nugraha *et al.*, 2022).

4.1.3. Lage Formation

The Pleistocene Lage Formation is composed of sandstones and mudstones with minor limestone intercalations. This formation is exposed mainly along the trans-Sulawesi highway in the Lage sub-district towards Tagolu village (Figs. 2 and 5E). Its total thickness estimated from measured sections is about 56 m. The maximum thickness of individual sections observed in road cuts is about 18 m. Two simple facies associations for the Lage Formation are offshore transition (FAL1) and slump deposits (FAL2).

4.1.3.1. Facies association Lage 1 (FAL1): offshore transition. The FAL1 facies association consists of thin-to medium-bedded sandstone and massive mudstone beds. The grey to brown sandstones have sub-rounded to sub-angular, very fine to coarse grains with good to moderate sorting. They are composed of grains of polycrystalline quartz (60%), monocrystalline quartz (10%), carbonate lithic (9%), metamorphic lithic (5%), serpentine (4%), sedimentary lithic (2%), potash feldspar (2%), plagioclase (1%), volcanic lithic (1%), and other accessory minerals (7%, e.g. chert, mica, and heavy minerals). Sedimentary structures of sandstone units in the FAL1 facies association include planar horizontal and wavy laminae. Bed thickness ranges from 3 to 120 cm. Mudstones are dark grey to dark brown, horizontally laminated and highly calcareous. Bioturbation is uncommon to moderate (bioturbation index is 2 to 3) and includes *Thalassinoides, Skolithos,* and *Rosselia* (Fig. 5F). Both mudstone and sandstone beds generally have planar upper and lower boundaries with an extensive sheet geometry. These beds generally have dips less than 5° to the west and are locally bioturbated. Interbedded grainstone (limestone) and mudstone occur in the upper part of the succession with a total thickness of 2 m.

The interbedded sandstones and mudstones of the FAL1 facies association were likely deposited in a clastic shelf environment up to 200 m deep based on the foraminifera assemblages that indicate an outer neritic environment (Nugraha *et al.*, 2022). Bioturbation and heavily weathered outcrops make sedimentary structures difficult to observe. Trace fossils of *Thalassinoides, Skolithos,* and *Rosselia* in mudstone beds indicate *Cruziana* ichnofacies in a distal lower shoreface to upper offshore environment (Pemberton *et al.*, 2012). Limestone and mudstone intercalations may be deposited during periods of low supply of terrigenous clastic detritus. The increasing proportion of sandstone upwards from mudstone to interbedded sandstone and mudstone may indicate an offshore transition from the offshore to shoreface.

4.1.3.2. Facies association Lage 2 (FAL2): slump. The FAL2 facies association is characterised by slumped conglomerate, sandstone, and mudstone beds that are confined between undisturbed FAL1 beds (Fig. 5E and G). The conglomerates are brown to grey, variably clast-to matrix-supported, with poor to moderate sorting. Clasts consist predominantly of sub-rounded to rounded quartz, metamorphic rocks, sandstones, siltstones, and limestones. The matrix comprises medium- to very-coarse grained sand. The conglomerate is interbedded with finely laminated fine-grained sediments. The fine-grained sediments comprise millimetre- to centimetre-thick interlaminations of mudstones, siltstones, and very fine-grained sandstones. The interbedded conglomerate and fine-grained sediments form asymmetric folds that are bounded by undisturbed FAL1 beds and dips moderately to the west. The total observed thickness from the top to base of the disturbed beds is about 4 m.

The FAL2 slump beds were associated with slope failure or gravity collapse. The reclined anticlines within the slumped bed generally verge towards the west, indicating the downslope direction (Nichols, 2009). Other instabilities were also possibly caused by a rapid or abrupt accumulation of conglomerate and a relatively denser pile of sediments onto wet and less dense muddy sediments. Thin laminations in the interbedded fine-grained sediments are indicative of tidal indicators. A coarsening-upward sequence within the slumped beds suggests that sediments were previously deposited in a shallower environment in a shelfal slope before they were remobilised and carried into a deeper water setting.

4.2. Mineralogical observations

4.2.1. Light minerals

Point counting was performed on six thin sections of the Puna Formation sandstones. Between 409 and 714 grains were counted in each thin section (Supplementary Data 3). They are predominantly serpentinite, potash feldspar, quartz, plagioclase feldspar, volcanic, and carbonate lithics (Fig. 6A and B). Other minerals include spinel, pyroxenes, and chlorite. Metamorphic lithic grains containing glaucophane were found in this formation (Fig. 6C). This also indicates that the sediments were derived locally from the Cretaceous and Oligo-Miocene metamorphic rocks.

Ternary sandstone classification (Fig. 6G) shows three feldspathic litharenites (ES13-263, ES14-42 and ES14-70), two litharenites (ES14-40 and ES13-271), and one arkose (ES14-80) sandstones. On the QFL plot (Fig. 6H), sample ES14-80 has a basement uplift provenance and other samples (ES13-263, ES13-271, ES14-40, ES14-42, and ES14-70) have a magmatic arc provenance. The QmFLt plot (Fig. 6I) suggests a basement uplift (ES14-80), lithic recycled (ES13-271 and ES14-40) and magmatic arc provenance (ES14-263, ES14-40 and ES14-42 and ES14-70).

The petrographic study of the Poso Formation indicates a composition of (1) micritic packstone, (2) packstone, and (3) wackestone microfacies (Supplementary File 4). Bioclastic components include benthic and planktonic foraminifera (Fig. 6D) which indicate outer neritic, fore reef, inner neritic, and shallow reefal environments.

The Lage Formation sandstone is a compositionally mature sublitharenite with predominant quartz grains (Fig. 6G). Predominant quartz, plagioclase, and glaucophane (Fig. 6E and F) have sub-angular to angular shapes, whereas lithic grains are sub-rounded to rounded. The glaucophane indicates a subduction-related source, derived locally from the Cretaceous and Oligo-Miocene metamorphic rocks. The QFL plot shows a recycled orogenic provenance and the QmFLt plot a lithic recycled provenance (Fig. 6H and I).

4.2.2. Heavy minerals

The Puna Formation (Fig. 7A—I; Supplementary Data 4) has predominant ultramafic and mafic grains that include pyroxenes (47.7%—24.7%), hornblende (48.0%—14.0%), and chrome spinel (17.7%—8.3%) indicating ultramafic and mafic rock sources. Garnet (5.0%—1.3%), epidote (3.7%), and titanite (2.3%) indicate a minor metamorphic rocks source. Surprisingly, zircon and glaucophane are not found in the heavy minerals from these samples, although glaucophane is present in lithic grains (see Section 4.2.1 above). The samples selected for heavy mineral analysis appears to be a bed that has no volcanic and blueschist material.

Sandstone from the Lage Formation (Fig. 7A and 7J-7Q; Supplementary Data 4) has a significant content of grains from metamorphic rocks, including glaucophane (24.3%), other amphiboles (14.7%), chlorite (5.7%), muscovite (4.3%), garnet (2.7%), lawsonite (2.7%), and tourmaline (2.0%). Glaucophane and lawsonite are characteristic of subduction-related high pressure-low temperature metamorphic rocks of the blueschist facies. Secondary sources include ultramafic and mafic rocks and ophiolite-rich sediment indicated by pyroxenes (18.0%), serpentine (12.0%), and chrome spinel (1.7%). A source of acid igneous rocks or metasedimentary rocks is shown by the presence of tourmaline (2.0%), zircon (1.7%), and apatite (1.0%).

4.2.3. Zircon geochronology

Zircons were not found in samples collected from the Puna Formation. Sample ES14-67 from the Lage Formation yielded a total of 138 zircon ages with a main late Cenozoic population and minor Permo-Triassic and Carboniferous populations (Fig. 8A; Supplementary Data 5). The Proterozoic zircons show a peak in the late Mesoproterozoic with minor grains of Palaeoproterozoic and Neoproterozoic age. The youngest grain from this sample is 3.5 ± 0.3 Ma which represents the maximum depositional age (Fig. 8B).

5. Discussion

5.1. Sedimentation history and provenance

The Puna Formation is interpreted to be the sedimentary product of an extensional asymmetric half-graben. The prograding deltas of Facies Association Puna 1 (FAP1) are exposed mainly in the eastern Poso Depression and were deposited in the hanging-wall of the graben (Fig. 9A). FAP1 is interpreted to have been deposited in the downslope part of a fan delta (e.g. Falk and Dorsey, 1998; Gobo *et al.*, 2015) during the Early Pliocene based on foraminifera and nannofossil assemblages (Nugraha *et al.*, 2022).

The light and heavy mineral analyses show a major ultramafic and basic rock source. This delta was supplied by an antecedent river that transported sediments from ultramafic and basic rocks of the East

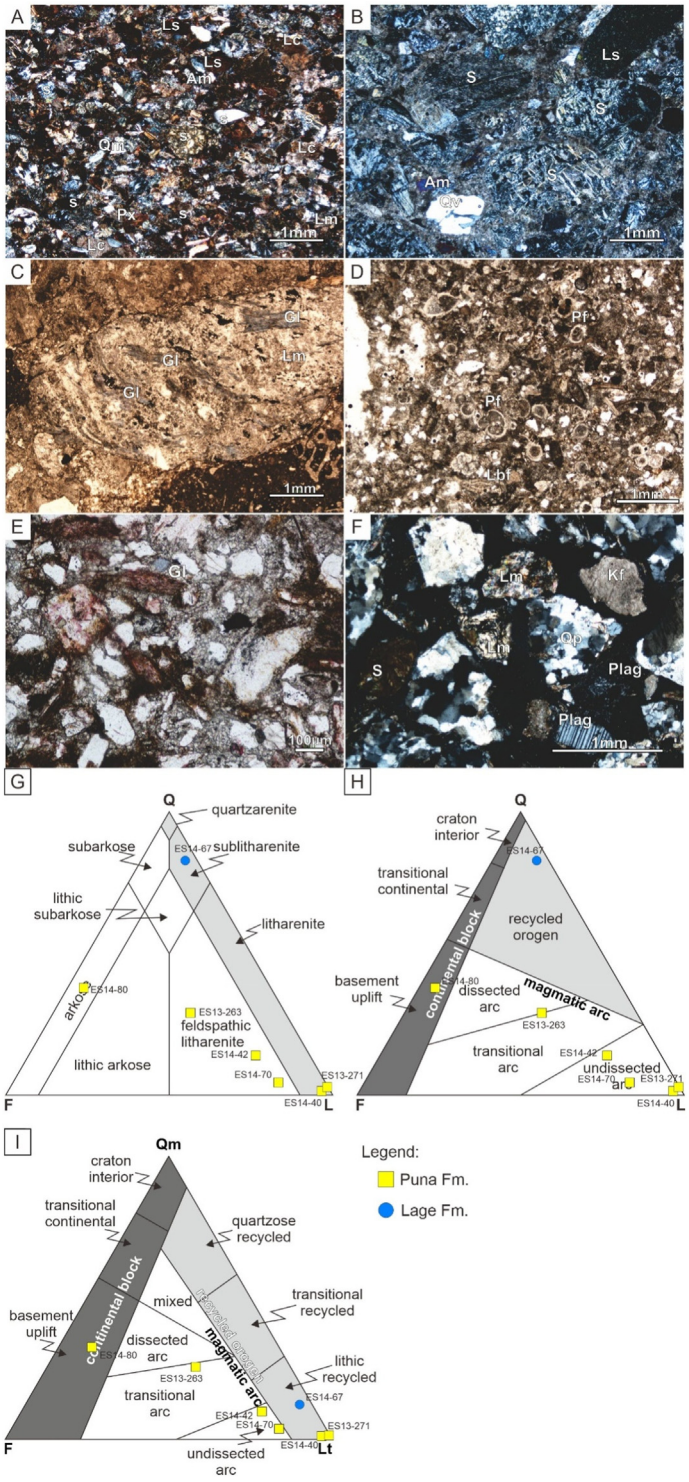

Fig. 6 Photomicrographs of **A**) litharenite in the Puna Formation (ES13-271, XPL) consists of predominant serpentinite (S), monocrystalline quartz (Qm), pyroxene (Px), sedimentary lithic (Ls), metamorphic lithic (Lm), and carbonate lithic (Lc); **B)** embayed volcanic quartz (Qv, ES14-47, XPL) and (**C**) metamorphic rock fragment (Lm) with glaucophane (Gl, ES14-77, PPL) in the Puna Formation (serpentinite (S), sedimentary lithic (Ls), Amphibole (Am)); **D)** wackestone of planktonic (Pf) and large benthic (Lbf) foraminifera (ES13-273 B, PPL); **E)** blue glaucophane (Gl), and; **F**) serpentinite (S), metamorphic lithic (Lm), polycrystalline quartz (Qp), potash feldspar (Kf), twinned and zoned plagioclase (Plag) in the Lage Formation (ES14-67); **G)** Q-F-L plot showing litharenite, feldspathic litharenite, and lithic arkose for the Puna Formation and sublitharenite for the Lage Formation; **H)** Q-F-L plot showing magmatic arc and basement uplift provenances for the Puna Formation and recycled orogen for the Lage Formation; **I)** Qm-F-Lt plot showing recycled orogens, magmatic arc, and basement uplift provenances for the Puna Formation and lithic recycled for the Lage Formation.

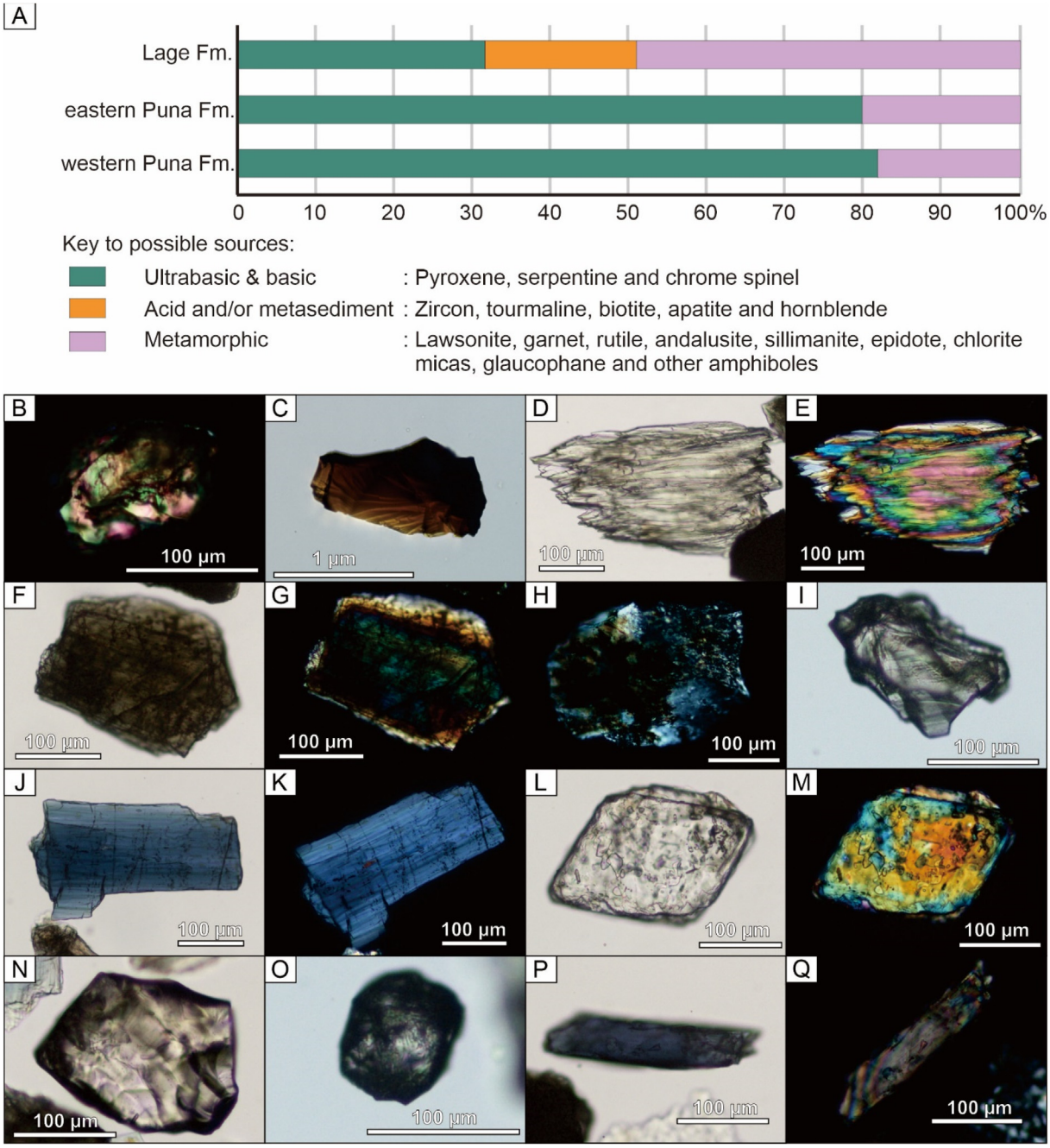

Fig. 7 **A)** Bar graph of possible source rocks for the Puna and Lage formations. Representative heavy minerals from the Puna Formation: (**B**) olivine, (**C**) chrome spinel, (**D-E**) pyroxene, (**F-G**) hornblende, (**H**) serpentine, and (**I**) garnet. From the Lage Formation: (**J-K**) glaucophane, (**L-M**) lawsonite, (**N**) garnet, (**O**) rounded zircon, (**P-Q**) blue tourmaline. White background is PPL and black background is XPL.

Sulawesi Ophiolite (ESO) in the east (Nugraha and Hall, 2018). Blueschist metamorphic lithics in the sandstones of the Puna Formation indicate subordinate sources were Cretaceous and Oligo-Miocene metamorphic rocks that are now exposed in the Tokorondo and Pompangeo Mountains respectively.

In the deepest parts of the basin, channel fill (FAP2) and levee complex (FAP3) facies associations were deposited contemporaneously. Conglomerates in the lower part of FAP2 indicate an initial influx of coarse-grained ultramafic-rich detritus. A wide textural range of conglomerates, from poorly- to well-sorted, both matrix-supported and clast-supported, indicates an early stage channel-complex set (e.g. Kneller *et al.*, 2020). Conglomerate clasts consist of predominant sub-rounded to rounded ultramafic and mafic rocks

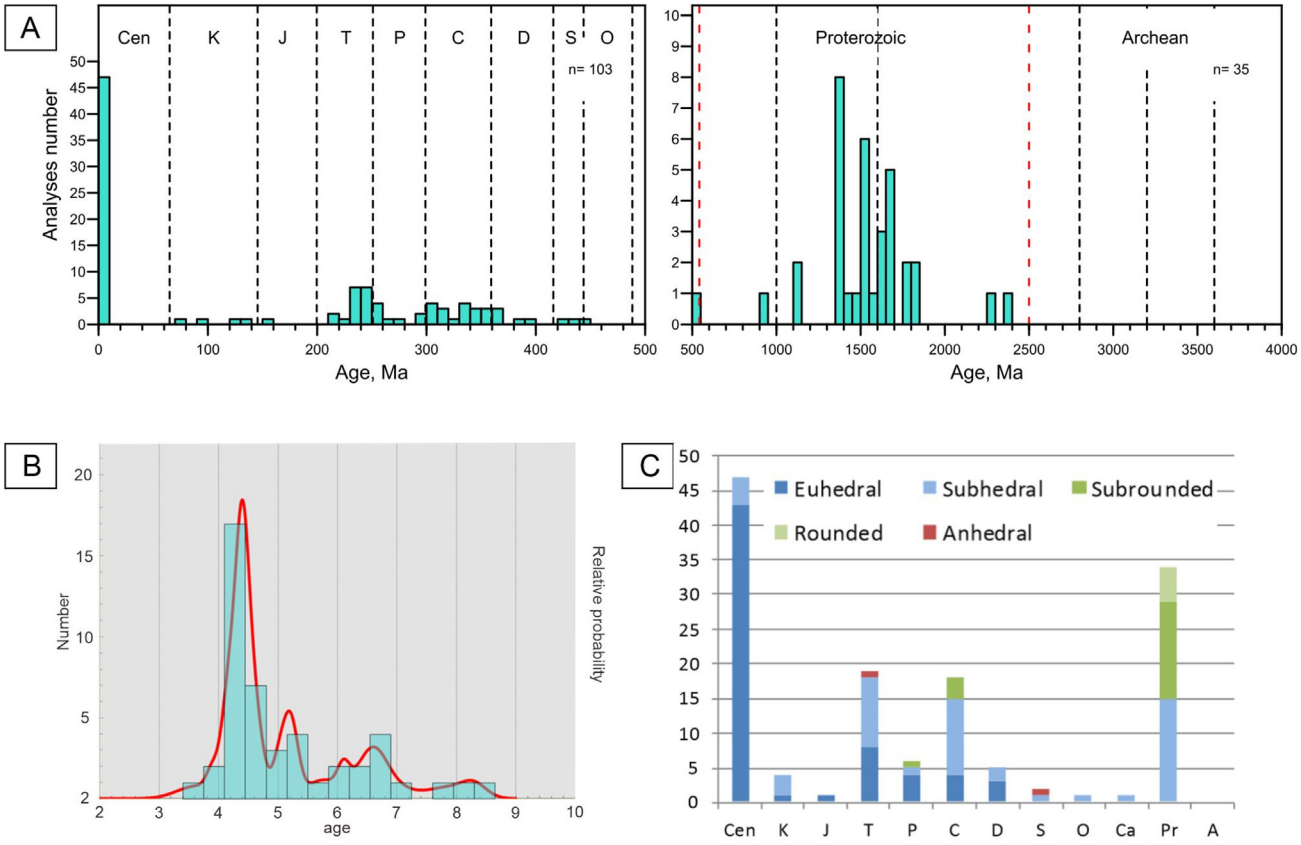

Fig. 8 **A)** Histograms showing concordant detrital zircon ages for the Lage Formation (sample ES13-257). Bin width for the Phanerozoic on the left (0—500 Ma) is 10 Ma and for the Precambrian on the right (500—4000 Ma) is 50 Ma. Cen abbreviation is for Cenozoic, K is for Cretaceous, J is for Jurassic, T is for Triassic, P is for Permian, C is for Carboniferous, D is for Devonian, S is for Silurian, O is for Ordovician; **B)** Detailed histogram for the Late Cenozoic concordant detrital zircon ages of the Lage Formation (sample ES13-257); **C)** Histogram of zircon morphology showing predominantly euhedral latest Miocene and Pliocene zircons.

(peridotite, basalt, and microgabbro) that were likely transported from the east. During this period (Fig. 9A and B) the Poso Depression was part of a seaway that connected Gorontalo Bay in the north and Bone Gulf in the south. A main submarine channel is interpreted along the basin axis where small submarine fans fed from the footwall and hangingwall highs. A long-lived north-south channel complex can also be observed today in Bone Bay (Camplin and Hall, 2014) and such a channel is a plausible modern analogue for the Puna Formation submarine channel in the Poso Depression.

The upper part of the Puna Formation is dominated by sandstone-rich channel-fill deposits (FAP2) and interbedded sandstone and mudstone of levee and overbank deposits (FAP3). The sandstone-rich unit of FAP2 indicates a deposition by debris flows and later reworking and winnowing by turbidity currents (Winn and Dott, 1979). Thicker sandstone beds are interpreted to have been deposited during a sand-rich, distributive stage of channel-complex development (Beaubouef, 2004). Sandstones from this succession contain predominant quartz, plagioclase, and potash feldspars that are indicative of a volcanic input. Plio-Pleistocene magmatism (ca 3.1 to 2.4 Ma) was reported from west Sulawesi granitoids that intrude metamorphic rocks of the PMC (Hennig *et al.*, 2017) and may have contributed igneous material to the Puna Formation. This magmatism was probably associated with metamorphism and exhumation of the Tokorondo Metamorphic Complex concurrent with significant uplift of the Tokorondo Mountains during this period (Fig. 9B). A general thinning- and fining-up succession of conglomerates through sandstone- and mudstone-dominated facies associations of the Puna Formation suggest progressive submarine channel abandonment. The increased main fault offset was probably responsible for the basin deepening in the Poso Depression. Sedimentary packages of slump, slide- and debris flow deposits reflect gravity-induced deposition that were likely caused by fault movements and earthquake activities (Fig. 9B). Deepening of the basin also coincided with arise in eustatic sea-

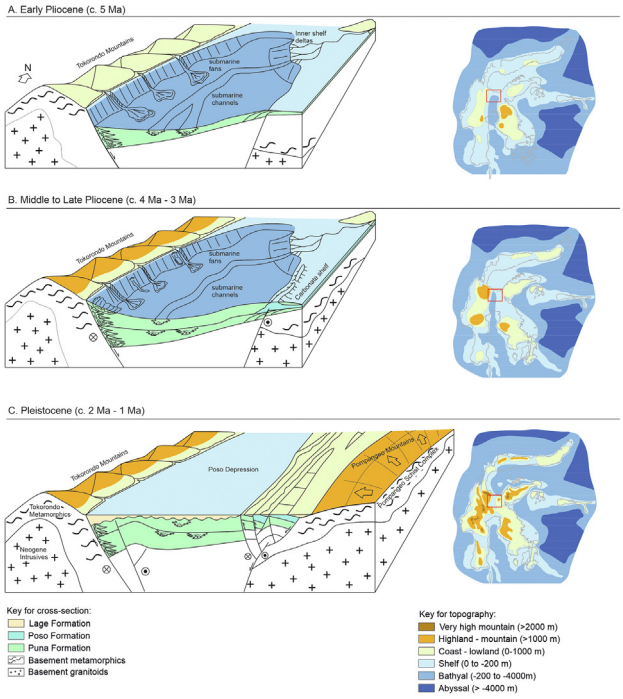

Fig. 9 Schematic 3D diagrams to summarise uplift and subsidence in Poso Depression, Tokorondo, and Pompangeo Mountains; **A)** Early Pliocene where uplift of the Tokorondo Mountains initiated subsidence in Poso Depression; **B)** Middle to Late Pliocene. Basin deepening is indicated by the fining-up Puna Formation. Sedimentary packages of interbedded debris flows, slide sheets, turbidites, and intermittent volcanic input within this formation reflect episodic movement during regional uplift. The carbonates of the Poso Formation were deposited on the hanging wall basin margin of an asymmetric basin; **C)** In the Pleistocene, increased exhumation the Pompangeo Schist Complex and its associated strike-slip faults deformed the Puna and Poso formations. Deposition of the Lage Formation records exhumation of the Pompangeo Schist Complex during the last 2 Ma.

level during the period from about 3.2 to 2.7 million years ago (Miller *et al.*, 2012; Steinthorsdottir *et al.*, 2020).

The carbonate platform of the Poso Formation developed on the crest of hanging wall blocks at the eastern margin of Poso Depression (Fig. 9B). We interpret it as a mixed shallow marine carbonate and siliciclastic depositional setting. Carbonates lying over fluvial topsets are common in many deltaic systems (e.g. Weimer, 1978; Coleman, 1981; Galloway and Hobday, 1996; Giosan and Bhattacharya, 2005; Backert *et al.*, 2010) and possibly developed during a period of low terrigenous input. The rudstone limestone above the stratigraphic contact between the Puna and Poso formations (Fig. 3) contains a Pliocene foraminifera assemblage (Nugraha *et al.*, 2022). This suggests a Pliocene or older age for the Puna Formation. However, the nature of conglomeratic-rudstone limestone suggests reworking of older material for the dated sample. If the dated sample was reworked, the Poso Formation has an age similar to the Puna Formation.

The Lage Formation was deposited in a shoreface to offshore transition during the early Pleistocene (Fig. 9C; 1.8—1 Ma, Nugraha *et al.*, 2022). Biostratigraphic ages from the Poso and Lage formations suggest a possible hiatus in the early Pleistocene (Nugraha *et al.*, 2022) and the change from steeply dipping carbonates of the Poso Formation (22°—82°) and almost horizontal beds of the Lage Formation (<5°) imply a tectonic cause. The change from carbonates of the Poso Formation to siliciclastics of the Lage Formation also indicates an increased sedimentation rate in the Poso Depression. The slumped beds are likely indicative of slope failure or gravity collapse due to earthquake activity and instabilities in a rapidly accumulated denser pile of sediments onto wet and less dense muddy sediments in a shelfal slope setting. The Lage Formation also records the exhumation of Oligo-Miocene subduction zone material based on the high proportion of euhedral glaucophane and lawsonite (Fig. 7). The main sediment source was the Pompangeo Schist Complex (PSC), from which glaucophane-bearing schists have been reported (Brouwer, 1934; de Roever, 1950, 1956). The exhumation of the PSC as part of a metamorphic core complex and movement on its detachment fault caused tilting and denudation in the eastern part of the Poso Depression up till present-day (Spencer, 2010, 2011). Detrital zircons from the Lage Formation record a main peak at Pliocene (ca 4.3 Ma, Fig. 8A and B) and youngest zircon age of 3.5 Ma ±0.3 Ma. The Latest Miocene and Pliocene euhedral zircons are probably derived from Neogene igneous rock sources in South, West, and Central Sulawesi (Fig. 8C; Polvé *et al.*, 1997; Elburg and Foden, 1999; Hennig *et al.*, 2017). The maximum depositional age of 3.5 Ma ±0.3 Ma supports the early Pleistocene depositional age for the Lage Formation. During this period, there were land bridges that connected West, East, and Southeast Sulawesi. The Poso Depression became a semi-enclosed shallow marine bay. Thereafter, the Poso Depression was fed mainly by the detrital sediments from the Tokorondo and Pompangeo metamorphic complexes and a gradually shallowing-up palaeoenvironment into a Quaternary fluvial and alluvial fan setting.

5.2. *Effects of changes in palaeogeography*

Most of the present relief of Sulawesi was created in the last 5 million years, and especially since 2 Myr, reflecting significant palaeogeographic changes in a geologically short time (Nugraha and Hall, 2018). There was a sea barrier in the Poso Depression separating landmasses that now form western and eastern Sulawesi from the Miocene to the Pliocene that likely hindered dispersal. A land bridge between eastern and western Sulawesi formed in the Late Pliocene (c. 3 Ma) and diminished biogeographic marine barriers to faunal distribution, particularly terrestrial faunas (e.g. Merker *et al.*, 2009; Frantz *et al.*, 2018; Hagemann *et al..*, 2022). This coincided with the eustatic sea-level fall after the Pliocene climatic optimum (Miller *et al.*, 2020). Sea barriers and land bridges are important for generating species endemism (e.g. Frantz *et al.*, 2018; Sin *et al.*, 2022). The palynological record from the Makassar Strait to the west of Sulawesi indicates equatorial ever-wet climates from the Late Miocene to Quaternary (Morley, 2012, 2018). The presence of ultramafic detritus in the Poso Depression implies long-lived elevated areas in eastern Sulawesi after ophiolite emplacement in the Early Miocene (Nugraha and Hall, 2018; Nugraha *et al.*, 2022). Rapid tectonic uplift and ultramafic lithologies in a tropical climate led to efficient chemical weathering and carbon sequestration in the Southeast Asian islands which likely contributed to global cooling associated with the expansion of northern hemisphere ice sheets for the Late Miocene and Pliocene (Shackleton *et al.*, 1984; Zachos *et al.*, 2001; Morley, 2012; Park *et al.*, 2020).

6. Conclusions

This outcrop-based sedimentological and provenance study identifies the sources and depositional environments of the Plio-Pleistocene sediments in the Poso Depression of Central Sulawesi. The Pliocene successions began with the deposition of the Puna Formation that includes coarse-grained fan deltas at the western basin margin and deep-water channel complexes in the basin deep. This formation was deposited in extensional asymmetric half-grabens. Provenance analyses show that sediments were sourced mainly from the ultrabasic rocks in East Sulawesi with intermittent magmatic and metamorphic input from West Sulawesi. Carbonates of the Poso Formation developed contemporaneously on the shallow marine eastern basin margin. They are unconformably overlain by shallow marine glaucophane-rich siliciclastics of the Pleistocene Lage Formation that record rapid Pompangeo Schist Complex (PSC) exhumation and uplift. The Poso Depression was initially a seaway between Gorontalo and Bone bays until the Pleistocene. A significant uplift of the PSC led to the formation of a land bridge connecting western and eastern Sulawesi. The increasing area of exposed land due to rapid tectonic uplift, as well as a tropical climate, likely contributed significantly to the faunal speciation and dispersal in Sulawesi and the surrounding region.

Brief introduction

Abang Mansyursyah Surya Nugraha obtained BSc geology from Institut Teknologi Bandung, Indonesia. He obtained MSc and PhD from the Royal Holloway University of London, UK where he joined the SE Asia Research Group. His PhD produced detailed Neogene geological history of Sulawesi based on integrated study of sedimentology, stratigraphy, paleontology, mineralogy, well, and seismic data. He is now working as a research fellow at the Earth Observatory of Singapore, Nanyang Technological University. His research interests include sedimentology and stratigraphy, sedimentary provenance, basin evolution, paleogeography, and tectonics.

Declaration of interest

The authors declare that they have no known competing financial interests or personal relationships that could have appeared to influence the work reported in this paper.

Acknowledgements

This study was supported by the SE Asia Research Group of Royal Holloway University of London, United Kingdom, which is backed by a consortium of oil companies. This research was also supported by the Earth Observatory of Singapore (EOS), Singapore and comprises EOS contribution number 508. Institut Teknologi Bandung and Benyamin Sapiie are thanked for making the fieldwork possible. Ekspedisi Poso and Universitas Pertamina are thanked for the later fieldwork supports. We thank Ramade and local guides for field assistance. Inga Sevastjanova is thanked for assistance with heavy mineral

separation. Martin Rittner is thanked for assistance with LA-ICP-MS U—Pb zircon analysis. Associate Editors-in-Chief Yuan Wang, and Santanu Banerjee, and an anonymous reviewer are thanked for their helpful review comments.

References

Abendanon, E.C., 1915. Central Celebes. *Geographical Journal*, 38, 594—598. https://doi.org/10.2307/1778843.

Albrecht, C., Stelbrink, B., Gauffre-Autelin, P., Marwoto, R.M., von Rintelen, T., Glaubrecht, M., 2020. Diversification of epizoic freshwater limpets in ancient lakes on Sulawesi, Indonesia: Coincidence or coevolution? *Journal of Great Lakes Research*, 46, 1187—1198. https://doi.org/10.1016/J.JGLR.2020.07.013.

Ali, J.R., Heaney, L.R., 2021. Wallace's line, Wallacea, and associated divides and areas: history of a tortuous tangle of ideas and labels. *Biological Reviews*, 96, 922—942. https://doi.org/10.1111/BRV.12683.

Andersen, T., 2002. Correction of common lead in U—Pb analyses that do not report 204Pb. *Chemical Geology*, 192, 59—79. https://doi.org/10.1016/S0009-2541(02)00195-X.

Andersen, T., 2005. Detrital zircons as tracers of sedimentary provenance: limiting conditions from statistics and numerical simulation. *Chemical Geology*, 216, 249—270. https://doi.org/10.1016/J.CHEMGEO.2004.11.013.

Audley-Charles, M.G., 1974. Sulawesi. In: Spencer, A.M. (Ed.), *Mesozoic-Cenozoic Orogenic Belts*, vol. 4. Geological Society of London Special Publication, pp. 365—378. https://doi.org/10.1144/GSL.SP.2005.004.01.21.

Backert, N., Ford, Ma, Malartre, F., 2010. Architecture and sedimentology of the Kerinitis Gilbert-type fan delta, Corinth Rift, Greece. *Sedimentology*, 57, 543—586. https://doi.org/10.1111/J.1365-3091.2009.01105.X.

Beaubouef, R.T., 2004. Deep-water leveed-channel complexes of the Cerro Toro Formation, Upper Cretaceous, southern Chile. *AAPG Bulletin*, 88, 1471—1500. https://doi.org/10.1306/06210403130.

Bernhardt, A., Jobe, Z.R., Lowe, D.R., 2011. Stratigraphic evolution of a submarine channel—lobe complex system in a narrow fairway within the Magallanes foreland basin, Cerro Toro Formation, southern Chile. *Marine and Petroleum Geology*, 28, 785—806. https://doi.org/10.1016/J.MARPETGEO.2010.05.013.

Brouwer, H.A., 1934. Geologische onderzoekingen op het eiland Celebes. *Kolonien Geologisch-Mijn-Bouwkundig Genootschap, Geology Series*, 10, 39—218.

Brouwer, H.A., Hetzel, W.H., Straeter, H.E.G., 1947. *Geological Explorations in the Island of Celebes*. North Holland Publishing Co., Amsterdam.

Camplin, D.J., Hall, R., 2014. Neogene history of Bone Gulf, Sulawesi, Indonesia. *Marine and Petroleum Geology*, 57, 88—108. https://doi.org/10.1016/J.MARPETGEO.2014.04.014.

Coleman, J.M., 1981. *Deltas. Processes of Deposition of Models for Exploration*. Burgess Publishing Company, Minneapolis.

Collinson, J., 1996. AlluvialSediments. In: Reading, H.G. (Ed.), *Sedimentary Environments: Processes, Facies and Stratigraphy*. Wiley, pp. 37—82.

Darlington, P.J., 1957. *Zoogeography: The Geographical Distribution of Animals*. John Wiley & Sons.

de Roever, W.P., 1950. Preliminary notes on glaucophane-bearing and other crystalline schists from South East Celebes, and on the origin of glaucophane-bearing rocks. *Nederlandsche Akademi Wetensch Proceedings*, 53, 1455—1456.

de Roever, W.P., 1956. Some additional data on the crystalline schists of the Rumbia and Mendoke Mountains, S.E. Celebes. Verhandelingen Koninklijk Nederlands Geologischen Mijnbouwkundig Genootschap. *Geologische Serie*, 16, 385—393.

Dickerson, R.E., Merrill, E.D., McGregor, R., Schultze, W., Taylor, E.H., Herre, A.W., 1928. *Distribution of Life in The Philippines*. In: *Monograph of the Bureau of Science*, vol. 21. Manila Bureau of Science.

Dickinson, W.R., 1970. Relations of andesites, granites, and derivative sandstones to arc-trench tectonics. *Reviews of Geophysics*, 8, 813—860. https://doi.org/10.1029/RG008I004P00813.

Dickinson, W.R., 1985. Interpreting provenance relations from detrital modes of sandstones. *Provenance of Arenites*, 333—361. https://doi.org/10.1007/978-94-017-2809-6_15.

Dickinson, W.R., Suczek, C.A., 1979. Plate tectonics and sandstone compositions. *AAPG Bulletin*, 63, 2164—2182. https://doi.org/10.1306/2F9188FB-16CE-11D7-8645000102C1865D.

Dickinson, W.R., Beard, L.S., Brakenridge, G.R., Erjavec, J.L., Ferguson, R.C., Inman, K.F., Knepp, R.A., Lindberg, F.A., Ryberg, P.T., 1983. Provenance of North American Phanerozoic sandstones in relation to tectonic setting. *Geological Society of America Bulletin*, 94, 222—235. https://doi.org/10.1130/0016-7606(1983)94<222:PONAPS>2.0.CO;2.

Dorsey, R.J., 1988. Provenance evolution and unroofing history of a modern arc-continent collision; evidence from petrography of Plio-Pleistocene sandstones, eastern Taiwan. *Journal of Sedimentary Research*, 58, 208—218. https://doi.org/10.1306/212F8D5A-2B24-11D7-8648000102C1865D.

Driller, C., Merker, S., Perwitasari-Farajallah, D., Sinaga, W., Anggraeni, N., Zischler, H., 2015. Stop and go — waves of tarsier dispersal mirror the genesis of Sulawesi Island. *PLOS ONE*, 10, e0141212. https://doi.org/10.1371/JOURNAL.PONE.0141212.

Elburg, M., Foden, J., 1999. Sources for magmatism in Central Sulawesi: geochemical and Sr—Nd—Pb isotopic constraints. *Chemical Geology*, 156, 67—93. https://doi.org/10.1016/S0009-2541(98)00175-2.

Evans, B.J., 2012. Coalescent-based analysis of demography: applications to biogeography on Sulawesi. In: Gower, D., Johnson, K., Richardson, J., Rosen, B., Rüber, L., Williams, S. (Eds.), *Biotic Evolution and Environmental Change in Southeast Asia 82*. Cambridge University Press, p. 270.

Evans, B.J., McGuire, J.A., Brown, R.M., Andayani, N., Supriatna, J., 2008. A coalescent framework for

comparing alternative models of population structure with genetic data: evolution of Celebes toads. *Biology Letters*, 4, 430—433. https://doi.org/10.1098/RSBL.2008.0166.

Evans, B.J., Brown, R.M., McGuire, J.A., Supriatna, J., Andayani, N., Diesmos, A., Iskandar, D., Melnick, D.J., Cannatella, D.C., 2003a. Phylogenetics of fanged frogs: Testing biogeographical hypotheses at the interface of the Asian and Australian faunal zones. *Systematic Biology*, 52, 794—819. https://doi.org/10.1093/SYSBIO/52.6.794.

Evans, B.J., Supriatna, J., Andayani, N., Melnick, D.J., 2003b. Diversification of Sulawesi Macaque Monkeys: Decoupled evolution of mitochondrial and autosomal DNA. *Evolution*, 57, 1931—1946. https://doi.org/10.1111/J.0014-3820.2003.TB00599.X.

Evans, B.J., Supriatna, J., Andayani, N., Setiadi, M.I., Cannatella, D.C., Melnick, D.J., 2003c. Monkeys and toads define areas of endemism on Sulawesi. *Evolution*, 57, 1436—1443. https://doi.org/10.1111/J.0014-3820.2003.TB00350.X.

Falk, P.D., Dorsey, R.J., 1998. Rapid development of gravelly high-density turbidity currents in marine Gilbert-type fan deltas, Loreto Basin, Baja California Sur, Mexico. *Sedimentology*, 45, 331—349. https://doi.org/10.1046/J.1365-3091.1998.0153E.X.

Fedo, C.M., Sircombe, K.N., Rainbird, R.H., 2003. Detrital zircon analysis of the sedimentary record. *Reviews in Mineralogy and Geochemistry*, 53, 277—303. https://doi.org/10.2113/0530277.

Fisher, R.V., 1971. Features of coarse-grained, high-concentration fluids and their deposits. *Journal of Sedimentary Research*, 41.

Frantz, L.A.F., Rudzinski, A., Nugraha, A.M.S., Evin, A., Burton, J., Hulme-Beaman, A., Linderholm, A., Barnett, R., Vega, R., Irving-Pease, E.K., Haile, J., Allen, R., Leus, K., Shephard, J., Hillyer, M., Gillemot, S., van den Hurk, J., Ogle, S., Atofanei, C., Thomas, M.G., Johansson, F., Mustari, A.H., Williams, J., Mohamad, K., Damayanti, C.S., Wiryadik, I.D., Obbles, D., Mona, S., Day, H., Yasin, M., Meker, S., McGuire, J.A., Evans, B.J., von Rintelen, T., Ho, S.Y.W., Searle, J.B., Kitchener, A.C., Macdonald, A.A., Shaw, D.J., Hall, R., Galbusera, P., Larson, G., 2018. Synchronous diversification of Sulawesi's iconic artiodactyls driven by recent geological events. *Proceedings of the Royal Society B: Biological Sciences*, 285. https://doi.org/10.1098/RSPB.2017.2566.

Galehouse, J.S., 1971. Point Counting. In: Carver, R.E. (Ed.), *Procedures in Sedimentary Petrology*, pp. 385—407.

Galloway, W., Hobday, D., 1996. *Terrigenous Clastic Depositional Systems: Applications to Fossil Fuel and Groundwater Resources*. Springer-Verlag, Berlin. https://doi.org/10.1007/978-3-642-61019-9.

Giosan, L., Bhattacharya, J.P., 2005. *River Deltas—Concepts, Models, and Examples*, vol. 83. SEPM Special Publication. https://doi.org/10.2110/PEC.05.83.

Gobo, K., Ghinassi, M., Nemec, W., 2015. Gilbert-type deltas recording short-term base-level changes: Delta-brink morphodynamics and related foreset facies. *Sedimentology*, 62, 1923—1949. https://doi.org/10.1111/SED.12212.

Griffin, W., Powell, W., Pearson, N., O'Reilly, S., 2008. *GLITTER: data reduction software for laser ablation ICP-MS, Laser Ablation-ICP-MS in the Earth Sciences*, vol. 40. Mineralogical Association of Canada Short Course Series, pp. 204—207.

Hagemann, L., Grow, N., Bohr, Y.E.M.B., Perwitasari-Farajallah, D., Duma, Y., Gursky, S.L., Merker, S., 2022. Small, odd and old: The mysterious Tarsiuspumilus is the most basal Sulawesi tarsier. *Biology Letters*, 18. https://doi.org/10.1098/RSBL.2021.0642.

Hall, R., 2012. Late Jurassic—Cenozoic reconstructions of the Indonesian region and the Indian Ocean. *Tectonophysics*, 570—571, 1—41. https://doi.org/10.1016/J.TECTO.2012.04.021.

Hall, R., Wilson, M.E.J., 2000. Neogene sutures in eastern Indonesia. *Journal of Asian Earth Sciences*, 18, 781—808. https://doi.org/10.1016/S1367-9120(00)00040-7.

Hamilton, W.B., 1979. *Tectonics of the Indonesian Region*, vol. 1078. U.S. Geological Survey Professional Paper, p. 345.

Hansen, L., Callow, R., Kane, I., Kneller, B., 2017. Differentiating submarine channel-related thin-bedded turbidite facies: Outcrop examples from the Rosario Formation, Mexico. *Sedimentary Geology*, 358, 19—34. https://doi.org/10.1016/J.SEDGEO.2017.06.009.

Heilprin, A., 1887. *The Geographical and Geological Distribution of Mammals*. Keegan Paul, Trench &Co, London.

Helmers, H., Sopaheluwakan, J., Nila, E.S., Tjokrosapoetro, S., 1989. Blueschist evolution is southeast Sulawesi, Indonesia. *Netherlands Journal of Sea Research*, 24, 373—381. https://doi.org/10.1016/0077-7579(89)90162-2.

Hennig, J., Hall, R., Forster, M.A., Kohn, B.P., Lister, G.S., 2017. Rapid cooling and exhumation as a consequence of extension and crustal thinning: Inferences from the Late Miocene to Pliocene Palu Metamorphic Complex, Sulawesi, Indonesia. *Tectonophysics*, 712—713, 600—622. https://doi.org/10.1016/J.TECTO.2017.06.025.

Hiscott, R.N., 1994. Loss of capacity, not competence, as the fundamental process governing deposition from turbidity currents. *Journal of Sedimentary Research*, 64, 209—214. https://doi.org/10.2110/JSR.64.209.

Hiscott, R.N., Pirmez, C., Flood, R.D., 1997. Amazon submarine fan drilling: A big step forward for deep-sea fan models. *Geoscience Canada*, 24, 13—24.

Hjellbakk, A., 1997. Facies and fluvial architecture of a high-energy braided river: the Upper Proterozoic Seglodden Member, Varanger Peninsula, northern Norway. *Sedimentary Geology*, 114, 131—161. https://doi.org/10.1016/S0037-0738(97)00075-4.

Holloway, J.D., Jardine, N., 1968. Two approaches to zoogeography: a study based on the distributions of butterflies, birds and bats in the Indo-Australian area. *Proceedings of the Linnean Society*, 179, 153—188.

Ingersoll, R.V., 1983. Petrofacies and provenance of Late Mesozoic forearc basin, Northern and Central California.

AAPG Bulletin, 67, 1125—1142. https://doi.org/10.1306/03B5B713-16D1-11D7-8645000102C1865D.

Kane, I.A., Kneller, B.C., Dykstra, M., Kassem, A., McCaffrey, W.D., 2007. Anatomy of a submarine channel—levee: An example from Upper Cretaceous slope sediments, Rosario Formation, Baja California, Mexico. *Marine and Petroleum Geology*, 24, 540—563. https://doi.org/10.1016/J.MARPETGEO.2007.01.003.

Kane, I.A., McCaffrey, W.D., Peakall, J., Kneller, B.C., 2010. Submarine channel levee shape and sediment waves from physical experiments. *Sedimentary Geology*, 223, 75—85. https://doi.org/10.1016/J.SEDGEO.2009.11.001.

Katili, J.A., 1978. Past and present geotectonic position of Sulawesi, Indonesia. *Tectonophysics*, 45, 289—322. https://doi.org/10.1016/0040-1951(78)90166-X.

Klompé, T.H.F., 1954. The structural importance of the Sula Spur (Indonesia). *Indonesian Journal of Natural Sciences*, 110, 21—40.

Kneller, B., 1995. *Beyond the turbidite paradigm: Physical models for deposition of turbidites and their implications for reservoir prediction*, vol. 94. Geological Society Special Publication, pp. 31—49. https://doi.org/10.1144/GSL.SP.1995.094.01.04.

Kneller, B.C., McCaffrey, W.D., 2003. The interpretation of vertical sequences in turbidite beds: The influence of longitudinal flow structure. *Journal of Sedimentary Research*, 73, 706—713. https://doi.org/10.1306/031103730706.

Kneller, B., Bozetti, G., Callow, R., Dykstra, M., Hansen, L., Kane, I., Li, P., McArthur, A., Catharina, A.S., Dos Santos, T., Thompson, P., 2020. Architecture, process, and environmental diversity in a late Cretaceous slope channel system. *Journal of Sedimentary Research*, 90, 1—26. https://doi.org/10.2110/JSR.2020.1.

Koolhoven, W.C.B., 1930. Verslag over eenverkenningstocht in den oostarm van Celebes en den Banggaiarchipel. JaarboekMijnwezenNederlandsch Oost Indië. *Verhandelingen*, 59, 127—152.

Kündig, E., 1956. *Geology and ophiolite problems of East Celebes*. Verhandelingen Koninklijk Nederlands Geologischen Mijnbouwkundig Genootschap Geologisch, pp. 210—234.

Lowe, D.R., 1982. Sediment gravity flows; II, Depositional models with special reference to the deposits of high-density turbidity currents. *Journal of Sedimentary Research*, 52, 279—297. https://doi.org/10.1306/212F7F31-2B24-11D7-8648000102C1865D.

Mange, M.A., Maurer, H.F.W., 1992. *Heavy Minerals in Colour*. Springer, Dordrecht. https://doi.org/10.1007/978-94-011-2308-2_7.

Mawaleda, M., Husain, J.R., Forster, M., Suparka, E., Abdullah, C.I., Basuki, N.I., Hutabarat, J., 2018. Miocene tectonic of the Southeast Arm of Sulawesi, Indonesia: Based on petrology data, geochemistry, and 40Ar/39Ar geochronology of metamorphic rocks from Rumbia Complex. *IOP Conference Series: Earth and Environmental Science*, 212, 012043. https://doi.org/10.1088/1755-1315/212/1/012043.

McCave, I.N., 1975. Vertical flux of particles in the ocean. *Deep-Sea Research and Oceanographic Abstracts*, 22, 491—502. https://doi.org/10.1016/0011-7471(75)90022-4.

Merker, S., Driller, C., Perwitasari-Farajallah, D., Pamungkas, J., Zischler, H., 2009. Elucidating geological and biological processes underlying the diversification of Sulawesi tarsiers. *Proceedings of the National Academy of Sciences*, 106, 8459—8464. https://doi.org/10.1073/PNAS.0900319106.

Merrill, E.D., 1924. The correlation of biological distribution with the geological history of Malaysia. In: Lightfoot, G. (Ed.), *Proceedings of the Pan-Pacific Science Congress, Australia*. Australian National Research Council, p. 1148, 1145.

Miall, A.D., 1977. A review of the braided-river depositional environment. *Earth-Science Reviews*, 13, 1—62. https://doi.org/10.1016/0012-8252(77)90055-1.

Miall, A.D., 1996. *The Geology of Fluvial Deposits: Sedimentary Facies, Basin Analysis, and Petroleum Geology*. Springer-Verlag Berlin Heidelberg, Germany, p. 598.

Miall, A.D., 2010. In: James, M.P., Dalrymple, R.W. (Eds.), *Facies Model*, 4. Geological Association of Canada, pp. 105—137.

Miall, A.D., 2014. *Fluvial Depositional Systems*. Springer International Publishing, Switzerland, p. 322.

Miall, A.D., Gibling, M.R., 1978. The Siluro-Devonian clastic wedge of Somerset Island, Arctic Canada, and some regional paleogeographic implications. *Sedimentary Geology*, 21, 85—127. https://doi.org/10.1016/0037-0738(78)90001-5.

Michaux, B., 1994. Land movements and animal distributions in east Wallacea (eastern Indonesia, Papua New Guinea and Melanesia). *Palaeogeography, Palaeoclimatology, Palaeoecology*, 112, 323—343. https://doi.org/10.1016/0031-0182(94)90079-5.

Miller, K.G., Wright, J.D., Browning, J.V., Kulpecz, A., Kominz, M., Naish, T.R., Cramer, B.S., Rosenthal, Y., Peltier, W.R., Sosdian, S., 2012. High tide of the warm Pliocene: Implications of global sea level for Antarctic deglaciation. *Geology*, 40, 407—410. https://doi.org/10.1130/G32869.1.

Miller, K.G., Browning, J.V., John Schmelz, W., Kopp, R.E., Mountain, G.S., Wright, J.D., 2020. Cenozoic sea-level and cryospheric evolution from deep-sea geochemical and continental margin records. *Science Advances*, 6. https://doi.org/10.1126/SCIADV.AAZ1346/SUPPL_FILE/AAZ1346_TABLE_S1.PDF.

Milsom, J., Ali, J., Sudarwono, S., 1999. Structure and collision history of the Buton Continental Fragment, eastern Indonesia. *AAPG Bulletin*, 83, 1320—1336. https://doi.org/10.1306/E4FD423D-1732-11D7-8645000102C1865D.

Mokodongan, D.F., Yamahira, K., 2015. Origin and intra-island diversification of Sulawesi endemic Adrianichthyidae. *Molecular Phylogenetics and Evolution*, 93, 150—160. https://doi.org/10.1016/J.YMPEV.2015.07.024.

Morley, R.J., 2012. A review of the Cenozoic palaeoclimate history of Southeast Asia. *Biotic Evolution and Environmental Change in Southeast Asia*, 79—114. https://doi.org/10.1017/CBO9780511735882.006.

Morley, R.J., 2018. Assembly and division of the South and South-East Asian flora in relation to tectonics and climate change. *Journal of Tropical Ecology*, 34, 209—234. https://doi.org/10.1017/S0266467418000202.

Mulder, T., Alexander, J., 2001. The physical character of subaqueous sedimentary density flows and their deposits. *Sedimentology*, 48, 269—299. https://doi.org/10.1046/J.1365-3091.2001.00360.X.

Müller, S., 1846. Ueber den charakter der thierwelt auf den Inseln des IndischenArchipels, einbeitragzurzoologischen-geographie. *Archiv für Naturgeschichte*, 12, 109—128.

Myers, N., Mittermeler, R.A., Mittermeler, C.G., Da Fonseca, G.A.B., Kent, J., 2000. Biodiversity hotspots for conservation priorities, 2000. *Nature*, 403(6772), 853—858. https://doi.org/10.1038/35002501, 403.

Nelson, D.R., 2001. An assessment of the determination of depositional ages for Precambrian clastic sedimentary rocks by U—Pb dating of detrital zircons. *Sedimentary Geology*, 141—142, 37—60. https://doi.org/10.1016/S0037-0738(01)00067-7.

Nemec, W., Steel, R.J., 1984. Alluvial and coastal conglomerates: Their significant features and some comments on gravelly mass-flow deposits. *Sedimentology of Gravels and Conglomerates — Memoir*, 10, 1—31.

Nichols, G., 2009. *Sedimentology and Stratigraphy*. Wiley-Blackwell, UK, p. 432pp.

Nugraha, A.M.S., Hall, R., 2018. Late Cenozoic palaeogeography of Sulawesi, Indonesia. *Palaeogeography, Palaeoclimatology, Palaeoecology*, 490, 191—209. https://doi.org/10.1016/J.PALAEO.2017.10.033.

Nugraha, A.M.S., Hall, R., BouDagher-Fadel, M., 2022. The Celebes Molasse: a revised Neogene stratigraphy for Sulawesi, Indonesia. *Journal of Asian Earth Sciences*, 228 . https://doi.org/10.1016/J.JSEAES.2022.105140.

O'Brien, N.R., 1996. *Shale lamination and sedimentary processes*, vol. 116. Geological Society Special Publication, pp. 23—36. https://doi.org/10.1144/GSL.SP.1996.116.01.04.

Park, Y., Maffre, P., Godderis, Y., MacDonald, F.A., Anttila, E.S.C., Swanson-Hysell, N.L., 2020. Emergence of the Southeast Asian islands as a driver for Neogene cooling. *Proceedings of the National Academy of Sciences of the United States of America*, 117, 25319—25326. https://doi.org/10.1073/PNAS.2011033117/-/DCSUPPLEMENTAL.

Parkinson, C.D., 1991. *The petrology, structure and geologic history of the metamorphic rocks of Central Sulawesi, Indonesia.*. PhD Thesis, University of London, p. 336pp.

Parkinson, C.D., 1996. The origin and significance of metamorphosed tectonic blocks in mélanges: evidence from Sulawesi, Indonesia. *Terra Nova*, 8, 312—323. https://doi.org/10.1111/J.1365-3121.1996.TB00564.X.

Parkinson, C., 1998. An outline of the petrology, structure and age of the Pompangeo Schist Complex of central Sulawesi, Indonesia. *Island Arc*, 7, 231—245. https://doi.org/10.1046/J.1440-1738.1998.00171.X.

Pearce, N.J.G., Perkins, W.T., Westgate, J.A., Gorton, M.P., Jackson, S.E., Neal, C.R., Chenery, S.P., 1997. A compilation of new and published major and trace element data for NIST SRM 610 and NIST SRM 612 glass reference materials. *Geostandards Newsletter*, 21, 115—144. https://doi.org/10.1111/J.1751-908X.1997.TB00538.X.

Pemberton, S.G., MacEachern, J.A., Dashtgard, S.E., Bann, K.L., Gingras, M.K., Zonneveld, J.P., 2012. Shorefaces. *Developments in Sedimentology*, 64, 563—603. https://doi.org/10.1016/B978-0-444-53813-0.00019-8.

Pezzati, G., Robert, H., Peter, B., Marta, P.-G., 2014. The Poso Basin in Gorontalo Bay, Sulawesi: Extension Related to Core Complex Formation on Land. Jakarta. In: *Indonesian Petroleum Association*, Proceedings 38th Annual Convention, p. IPA14. G-297 1—12.

Pickering, K., Coleman, J., Cremer, M., Droz, L., Kohl, B., Normark, W., O'Connell, S., Stow, D., Meyer-Wright, A., 1986. A high sinuosity, laterally migrating submarine fan channel-levee-overbank: results from DSDP Leg 96 on the Mississippi Fan, Gulf of Mexico. *Marine and Petroleum Geology*, 3, 3—18. https://doi.org/10.1016/0264-8172(86)90052-8.

Polvé, M., Maury, R.C., Bellon, H., Rangin, C., Priadi, B., Yuwono, S., Joron, J.L., SoeriaAtmadja, R., 1997. Magmatic evolution of Sulawesi (Indonesia): constraints on the Cenozoic geodynamic history of the Sundaland active margin. *Tectonophysics*, 272, 69—92. https://doi.org/10.1016/S0040-1951(96)00276-4.

Postma, G., Nemec, W., Kleinspehn, K.L., 1988. Large floating clasts in turbidites: a mechanism for their emplacement. *Sedimentary Geology*, 58, 47—61. https://doi.org/10.1016/0037-0738(88)90005-X.

Procheș, Ș., Ramdhani, S., 2012. The world's zoogeographical regions confirmed by cross-taxon analyses. *BioScience*, 62, 260—270. https://doi.org/10.1525/BIO.2012.62.3.7.

Rusmana, E., Sukido, Sukarna, D., Haryanto, E., Simandjuntak, T.O., 1993. *Geological Map of the Lasusua - Kendari Quadrangles (Quadrangles 2112, 2212), Sulawesi, Scale 1:250,000*. Bandung, Indonesia.

Sarasin, P., Sarasin, F., 1901. *MaterialienzurNaturgeschichte der Insel Celebes. Vierter Band: EntwurfeinerGeografisch-GeologischenBeschreibung der Insel Celebes*. G.W. Kreidel's Verlag, Wiesbaden, Germany.

Sclater, W.L., Scalater, P.L., 1899. *The Geography of Mammals*. Kegan Paul, Trench, Trübner& Co. Ltd, London.

Shackleton, N.J., Backman, J., Zimmerman, H., Kent, D.V., Hall, M.A., Roberts, D.G., Schnitker, D., Baldauf, J.G., Desprairies, A., Homrighausen, R., Huddlestun, P., Keene, J.B., Kaltenback, A.J., Krumsiek, K.A.O., Morton, A.C., Murray, J.W., Westberg-Smith, J., 1984. Oxygen isotope calibration of the onset of ice-rafting and history of glaciation in the North Atlantic region, 1984. *Nature*, 307(5952), 620—623. https://doi.org/10.1038/307620a0, 307.

Shanmugam, G., 1997. The Bouma Sequence and the turbidite mind set. *Earth-Science Reviews*, 42, 201—229. https://doi.org/10.1016/S0012-8252(97)81858-2.

Shanmugam, G., 2000. 50 years of the turbidite paradigm (1950s—1990s): deep-water processes and facies models—a critical perspective. *Marine and Petroleum Geology*, 17, 285—342. https://doi.org/10.1016/S0264-8172(99)00011-2.

Simandjuntak, T.O., Surono, Supandjono, J.B., 1997. *Geological map of the Poso quadrangle, Sulawesi quadrangle 2115, Scale 1: 250,000*. Bandung, Indonesia.

Sin, Y.C.K., Kristensen, N.P., Gwee, C.Y., Chisholm, R.A., Rheindt, F.E., 2022. Bird diversity on shelf islands does not benefit from recent land-bridge connections. *Journal of Biogeography*, 49, 189—200. https://doi.org/10.1111/JBI.14293.

Sláma, J., Košler, J., Condon, D.J., Crowley, J.L., Gerdes, A., Hanchar, J.M., Horstwood, M.S.A., Morris, G.A., Nasdala, L., Norberg, N., Schaltegger, U., Schoene, B., Tubrett, M.N., Whitehouse, M.J., 2008. Plešovice zircon — A new natural reference material for U—Pb and Hf isotopic microanalysis. *Chemical Geology*, 249, 1—35. https://doi.org/10.1016/J.CHEMGEO.2007.11.005.

Spencer, J.E., 2010. Structural analysis of three extensional detachment faults with data from the 2000 Space-Shuttle Radar Topography Mission. *GSA Today*, 20, 4—10. https://doi.org/10.1130/GSATG59A.1.

Spencer, J.E., 2011. Gently dipping normal faults identified with Space Shuttle radar topography data in central Sulawesi, Indonesia, and some implications for fault mechanics. *Earth and Planetary Science Letters*, 308, 267—276. https://doi.org/10.1016/J.EPSL.2011.06.028.

Steinthorsdottir, M., Coxall, H.K., de Boer, A.M., Huber, M., Barbolini, N., Bradshaw, C.D., Burls, N.J., Feakins, S.J., Gasson, E., Henderiks, J., Holbourn, A.E., Kiel, S., Kohn, M.J., Knorr, G., Kürschner, W.M., Lear, C.H., Liebrand, D., Lunt, D.J., Mörs, T., Pearson, P.N., Pound, M.J., Stoll, H., Strömberg, C.A.E., 2021. The Miocene: The future of the past. *Paleoceanography and Paleoclimatology*, 36, e2020PA004037. https://doi.org/10.1029/2020PA004037.

Stelbrink, B., Albrecht, C., Hall, R., von Rintelen, T., 2012. The biogeography of Sulawesi revisited: Is there evidence for a vicariantorigin of taxa on Wallace's "Anomalous Island". *Evolution*, 66, 2252—2271. https://doi.org/10.1111/J.1558-5646.2012.01588.X.

Sukamto, R., 1975. The structure of Sulawesi in the light of plate tectonics. In: Wiryosujono, S., Sudradjat, A. (Eds.), *Proceedings of the Regional Conference on the Geology and Mineral Resources of Southeast Asia*. Indonesian Association of Geologists, Jakarta, Indonesia, pp. 12—141.

Sukamto, R., Simandjuntak, T.O., 1983. Tectonic relationship between geologic provinces of western Sulawesi, eastern Sulawesi and Banggai-Sula in the light of sedimentological aspects. *Bulletin of the Geological Research and Development Centre*, 7, 1—12.

Surlyk, F., 1978. Submarine fan sedimentation along fault scarps on tilted fault blocks (Jurassic- Cretaceous boundary, E. Greenland). *Bulletin Grønland sGeologiske Undersøgelse*, 128, 108.

Vaillant, J.J., Haffner, G.D., Cristescu, M.E., 2011. The ancient lakes of Indonesia: Towards integrated research on speciation. *Integrative and Comparative Biology*, 51, 634—643. https://doi.org/10.1093/ICB/ICR101.

van Bemmelen, R.W., 1949. *The Geology of Indonesia*, IA. General Geology of Indonesia and Adjacent Archipelagos. Government Printing Office, Nijhoff, The Hague.

van Den Bergh, G.D., De Vos, J., Sondaar, P.Y., 2001. The Late Quaternary palaeogeography of mammal evolution in the Indonesian Archipelago. *Palaeogeography, Palaeoclimatology, Palaeoecology*, 171, 385—408. https://doi.org/10.1016/S0031-0182(01)00255-3.

van Welzen, P.C., Slik, J.F., Alahuhta, J., 2003. *Plant distribution patterns and plate tectonics in Malesia. In Plant diversity and complexity patterns: local, regional and global dimensions*. In: Proceedings of an International Symposium Held at the Royal Danish Academy of Sciences and Letters in Copenhagen, Denmark, 25-28 May, pp. 199—217.

Villeneuve, M., Gunawan, W., Cornee, J.J., Vidal, O., 2001. Geology of the central Sulawesi belt (eastern Indonesia): constraints for geodynamic models, 2001. *International Journal of Earth Sciences*, 91(3 91), 524—537. https://doi.org/10.1007/S005310100228.

von Rintelen, K., Cai, Y., 2009. Radiation of endemic species flocks in ancient lakes: systematic revision of the freshwater shrimp Caridina H. Milne Edwards, 1837 (Crustacea: Decapoda: Atyidae) from the ancient lakes of Sulawesi, Indonesia, with the description of eight new species. *Raffles Bulletin of Zoology*, 57, 343—452.

von Rintelen, K., von Rintelen, T., Glaubrecht, M., 2007. Molecular phylogeny and diversification of freshwater shrimps (Decapoda, Atyidae, Caridina) from ancient Lake Poso (Sulawesi, Indonesia)—The importance of being colourful. *Molecular Phylogenetics and Evolution*, 45, 1033—1041. https://doi.org/10.1016/J.YMPEV.2007.07.002.

Wallace, A.R., 1860. On the zoological geography of the Malay Archipelago. *Zoology*, 4, 172—184. https://doi.org/10.1111/j.1096-3642.1860.tb00090.x.

Wallace, A.R., 1863. On the physical geography of the Malay Archipelago. *Journal of the Royal Geographical Society of London*, 33, 217—234.

Wallace, A.R., 1869. *The Malay Archipelago*. Macmillan and Co., London.

Wallace, A.R., 1876. Lecture on the Comparative Antiquity of Continents, as Indicated by the Distribution of Living and Extinct Animals. *Proceedings of the Royal Geographical Society of London*, 21, 505. https://doi.org/10.2307/1799925.

Watkinson, I.M., 2011. Ductile flow in the metamorphic rocks of Central Sulawesi. In: Hall, R., Cottam, M.A., Wilson, M.E.J. (Eds.), *The SE Asian Gateway: History and Tectonics of the Australia-Asia Collision*, vol. 355. Geological Society of London Special Publication, pp. 157—176. https://doi.org/10.1144/SP355.8.

Weimer, R.J., 1978. Deltaic and shallow marine sandstones: sedimentation, tectonics and petroleum occurrences. In: *AAPG Continuing Education, Course Note Series 2*. American Association of Petroleum Geologists, Tulsa, OK, United States, pp. 1—167.

Wijbrans, J.R., Helmers, H., Sopaheluwakan, J., 1994. The age and thermal evolution of blueschists from southeast Sulawesi, Indonesia: the case of slowly cooled phengites. *Mineralogical Magazine*, 58A, 975—976. https://doi.org/10.1180/MINMAG.1994.58A.2.242.

Wilson, J.L., 1975. *Principles of Carbonate Sedimentation, Carbonate Facies in Geologic History*. Springer, New

York, NY. https://doi.org/10.1007/978-1-4612-6383-8_1.

Winn, R.D., Dott, R.H., 1979. Deep-water fan-channel conglomerates of Late Cretaceous age, southern Chile. *Sedimentology*, 26, 203—228. https://doi.org/10.1111/J.1365-3091.1979.TB00351.X.

Zachos, J., Pagani, H., Sloan, L., Thomas, E., Billups, K., 2001. Trends, rhythms, and aberrations in global climate 65 Ma to present. *Science*, 292, 686—693. https://doi.org/10.1126/SCIENCE.1059412/SUPPL_FILE/INDEX.HTML.

Appendix A. Supplementary data

Supplementary data to this article can be found online at https://doi.org/10.1016/j.jop.2023.05.003.